

OPTIMIZING THE MECHANICAL DESIGN
OF AN UNTETHERED ANKLE EXOSKELETON

By

James Babers

A Thesis

Submitted in Partial Fulfillment

of the Requirements for the Degree of

Master of Science

in Mechanical Engineering

Northern Arizona University

May 2020

Approved:

Zachary Lerner, Ph.D., Chair

F. Ernesto Penado, Ph.D.

David Trevas, Ph.D.

ABSTRACT

OPTIMIZING THE MECHANICAL DESIGN OF AN UNTETHERED ANKLE EXOSKELETON

JAMES BABERS

Ankle exoskeletons are wearable robotic devices designed to improve mobility in individuals with conditions that cause gait impairment, such as cerebral palsy or stroke. They accomplish this by providing ankle joint torque to the user. This torque assists in plantarflexion during the propulsive phase of gait or dorsiflexion during the clearance phase of gait. Exoskeleton studies have demonstrated promising results in these populations but many of the devices used in these studies have not benefited from significant efforts to optimize mechanical design for device performance.

This thesis presents the mechanical design, manufacture, and validation of an optimized, untethered ankle exoskeleton. The design process utilized a prototype device as an initial platform and optimized materials and design features to improve device performance. The high potential for optimization of the prototype device was clear, as the device utilized sound, system-level design approaches but had several design, material, and manufacturing shortcomings. An additional goal of this thesis is to provide a resource for future optimization efforts.

Validation showed that the optimized device met performance goals in the criteria of mass, torque tracking, ergonomics, and durability. These results indicate high potential for use of the optimized exoskeleton device in clinical studies and research applications.

Acknowledgments

I would like to thank my advisor Dr. Zachary Lerner for his support and guidance throughout my graduate work. He gave me the opportunity to pursue interesting projects that help people and for that I will always be thankful.

I would also like to thank my committee members Dr. F. Ernesto Penado and Dr. David Trevas for volunteering their time and effort to support my thesis defense.

Finally, I would like to thank the members of Northern Arizona University's Biomechatronics Lab, who were always helpful and kind.

Contents

ABSTRACT.....	ii
List of Tables	vii
List of Figures	viii
Chapter 1 Introduction and Background	1
Chapter 2 Literature Review	3
2.1 Sawicki Passive Exoskeleton.....	3
2.2 Harvard Exosuit	5
2.3 Collins Tethered Exoskeleton.....	7
2.4 Herr Ankle Exoskeleton	9
2.5 Original Lerner Exoskeleton	11
Chapter 3 System Level Design Criteria	15
3.1 Device Mass.....	15
3.2 Ergonomics.....	16
3.3 Durability.....	17
3.4 Torque Tracking.....	18
Chapter 4 Design Concepts	20
4.1 System Overview.....	20
4.2 Footplate	21

4.3	Lower Leg Assembly	32
4.4	Motor Assembly	41
Chapter 5 Validation		46
5.1	Validation Protocol.....	46
5.2	Device Mass	47
5.3	Torque Tracking	49
5.4	Ergonomics	52
5.5	Durability	55
Chapter 6 Manufacturing		56
6.1	Motor Assembly	56
6.1.1	Motor Panels.....	56
6.1.2	Chain and Sprocket	57
6.2	Lower Leg Assembly	58
6.2.1	Footplate and Shank Interface Components	58
6.2.2	Ankle Pulley and Bowden Cable Brackets.....	60
6.2.3	Carbon Fiber Support Tube.....	61
Chapter 7 Future Work		63
7.1	Telescoping Support Tube.....	63
7.2	Quick-Disconnect Bowden Cable	64

7.3	Alternative Carbon Fiber Layup Methods	65
7.3.1	Prepreg Carbon Fiber	65
7.3.2	Vacuum Infusion Layup.....	65
Chapter 8	Conclusions	66
References	68

List of Tables

TABLE 1: DISTAL MASS, TOTAL MASS, AND PEAK PLANTARFLEXION TORQUE [7],[25],[20],[17].....	48
TABLE 2: RMSE, VARIOUS WALKING CONDITIONS, OPTIMIZED DEVICE.....	51

List of Figures

FIGURE 1: SAWICKI PASSIVE DEVICE (PROFILE VIEW) [20]	3
FIGURE 2: SAWICKI PASSIVE DEVICE (REAR VIEW) [20].....	3
FIGURE 3: EXOSUIT SHANK INTERFACE [17]	6
FIGURE 4: EXOSUIT [17]	6
FIGURE 5: (B): ALPHA DESIGN (C): BETA DESIGN [15]	8
FIGURE 6: INITIAL HERR DEVICE [8].....	10
FIGURE 7: OPTIMIZED HERR DEVICE [25].....	10
FIGURE 8: ORIGINAL LERNER EXOSKELETON [7]	12
FIGURE 9: NET METABOLIC RATE VS LOAD [29]	15
FIGURE 10: A SHORT SHANK INTERFACE (RIGHT) CREATES LARGER TORQUE REACTION FORCES AND GREATER SOFT TISSUE COMPRESSION [18]	16
FIGURE 11: PASSIVE EXOSKELETON WITH SIGNIFICANT POSTERIOR PROTRUSION [32]	17
FIGURE 12: TORQUE TRACKING, MEASURE AND DESIRED VS TIME [15]	18
FIGURE 13: ORIGINAL LERNER EXOSKELETON [7]	21
FIGURE 14: OPTIMIZED EXOSKELETON	21
FIGURE 15: ORIGINAL LERNER FOOTPLATE [7].....	22
FIGURE 16: OPTIMIZED FOOTPLATE.....	22
FIGURE 17: STRESS IN SHOULDER, OPTIMIZED FOOTPLATE	23
FIGURE 18: STRESS IN SHOULDER, ORIGINAL LERNER FOOTPLATE.....	23
FIGURE 19: LATERAL SUPPORT MOMENT.....	24
FIGURE 20: ROTATIONAL DEFLECTION, ORIGINAL LERNER FOOTPLATE	25

FIGURE 21: ROTATIONAL DEFLECTION, OPTIMIZED FOOTPLATE	25
FIGURE 22: FRONTAL PLANE DEFLECTION, OPTIMIZED FOOTPLATE.....	26
FIGURE 23: FRONTAL PLANE DEFLECTION, ORIGINAL LERNER FOOTPLATE.....	26
FIGURE 24: MOMENT GENERATION ABOUT FOREFOOT [15].....	27
FIGURE 25: SELF-SUPPORTING OPTIMIZED ASSEMBLY	27
FIGURE 26: CURVED FOREFOOT GEOMETRY DURING PROPULSIVE GAIT PHASE	28
FIGURE 27: SHORT FOOTPLATE DESIGN [21].....	29
FIGURE 28: HIGH DISTAL MASS DEVICE [8]	30
FIGURE 29: FIBER-REINFORCED 3D PRINTED FOOTPLATE	31
FIGURE 30: STRUT DESIGN FOOT INTERFACE	31
FIGURE 31: NON-SELF-SUPPORTING DEVICE [15]	32
FIGURE 32: ORIGINAL LERNER LOWER LEG ASSEMBLY [7].....	33
FIGURE 33: OPTIMIZED LOWER LEG ASSEMBLY	33
FIGURE 34: DEVICE WITH SHORT SHANK INTERFACE SUPPORTS [18]	35
FIGURE 35: MOMENT ARM, COTS TORQUE SENSOR, CANTILEVERED DESIGN [34].....	36
FIGURE 36: MOMENT ARM, OPTIMIZED EXOSKELETON	36
FIGURE 37: BEARING CONFIGURATION, OPTIMIZED EXOSKELETON	37
FIGURE 38: BOWDEN CABLE AND ANKLE PULLEY ALIGNMENT, OPTIMIZED EXOSKELETON	38
FIGURE 39: PLANTARFLEXION-ONLY DEVICE [20].....	39
FIGURE 40: AN INTERMEDIATE LOWER LEG CONFIGURATION	40
FIGURE 41: INTERMEDIATE DESIGN, 3D PRINTED PULLEY	40
FIGURE 42: MOTOR ASSEMBLY (PARTIALLY DISASSEMBLED), OPTIMIZED EXOSKELETON	41

FIGURE 43: SPOOL AND TENSIONER CONFIGURATION, ORIGINAL LERNER EXOSKELETON	43
FIGURE 44: STRIPPED BOWDEN CABLE.....	44
FIGURE 45: DISTAL VS TOTAL MASS OF LEADING ANKLE EXOSKELETONS.....	47
FIGURE 46: DISTAL MASS VS PEAK PLANTARFLEXION TORQUE OF LEADING EXOSKELETONS.....	48
FIGURE 47: TOTAL MASS VS PEAK PLANTARFLEXION TORQUE OF LEADING EXOSKELETONS	49
FIGURE 48: PRESCRIBED VS MEASURED TORQUE, CLOSE LOOP, OPTIMIZED EXO.....	50
FIGURE 49: TORQUE VS RMSE, ALL CONFIGURATIONS	51
FIGURE 50: OPTIMIZED AND ORIGINAL EXO RMSE VALUES.....	52
FIGURE 51: SHANK INTERFACE ROTATION ABOUT TIBIAL AXIS.....	53
FIGURE 52: SHANK INTERFACE TRANSLATION MAGNITUDE	54
FIGURE 53: SHANK INTERFACE ROTATION IN THE SAGITTAL PLANE	54
FIGURE 54: TORQUE PROFILE.....	55
FIGURE 55: MOTOR PANEL, OPTIMIZED EXOSKELETON.....	57
FIGURE 56: CHAIN AND SPROCKET TRANSMISSION SYSTEM, OPTIMIZED EXOSKELETON	57
FIGURE 57: INTERLOCKING 3D PRINTED FOOTPLATE MOLDS.....	58
FIGURE 58: INTERLOCKING 3D PRINTED SHANK INTERFACE MOLDS.....	59
FIGURE 59: EIGER PRINTING ORIENTATION, ANKLE PULLEY.....	61
FIGURE 60: EIGER PRINTING ORIENTATION, BOWDEN CABLE BRACKET	61
FIGURE 61: CARBON FIBER REINFORCEMENT SPECIFICATION, ANKLE PULLEY	61
FIGURE 62: STEPCRAFT CNC	62
FIGURE 63: RIGID WET TILE SAW	62
FIGURE 64: TELESCOPING CARBON FIBER TUBES.....	63

FIGURE 65: QUICK-DISCONNECT BRACKET MOCK-UP 64

Chapter 1 Introduction and Background

Individuals with neurological disorders such as cerebral palsy and stroke can experience walking impairment and a subsequent reduction in mobility [1],[2],[3]. These disorders can cause spasticity and reduce selective motor control and strength, leading to gait deviations and decreased walking metabolic efficiency [4],[5],[6].

Wearable robotic devices, commonly referred to as exoskeletons, have been shown to improve metabolic efficiency of walking in healthy individuals and individuals with cerebral palsy, as well as improve gait patterns in post-stroke walking [7],[8],[9]. These devices reduce metabolic demand by providing assistive joint torque throughout the gait cycle in a profile reflective of the user's own biological joint torque [7]. They have also shown potential as rehabilitative training tools, improving muscular coordination and activity-specific strength through resistive, rather assistive, training [10].

Common interventions to improve mobility in these populations such as physical therapy, ankle-foot-orthoses (AFOs), and orthopedic surgery have shown limited success and can have significant drawbacks [11],[12],[13],[14]. The potential for wearable robotic devices to improve mobility outcomes in these populations is high, particularly if these devices are optimized for performance.

Much of the progress in exoskeleton research is relatively recent. Consequently, the devices used in many exoskeleton studies could be aptly characterized as prototype or first-generation designs [15],[16],[7]. A 2018 study by Lerner et al. in particular, specifically stated that the mechanical

design was not optimized for material selection but instead prioritized ease of fabrication for their feasibility study [7]. A paper by Walsh et al. presented an optimized version of an earlier device, but the weight only decreased from 4.09kg per leg assisted to 3.8kg per leg assisted, a device mass which is still far too high for optimal performance [9],[17].

These and other devices have significant shortcomings which limit their performance and diminish their research and clinical potential. While an in-depth review of several leading exoskeleton devices is presented in chapter two, the following are some primary shortcomings of many of these devices: tethered designs which can only be used for treadmill walking in research settings, impractically heavy components which impart significant metabolic demand, comfort issues which can limit user walking time, ergonomic issues which negatively affect gait patterns and create terrain restrictions, and design approaches which are only effective for a narrow range of users or have inherently limited performance potential [15],[8],[9],[17],[18],[19],[20],[7].

This thesis presents the mechanical design, validation, and manufacturing methods of an optimized ankle exoskeleton that meets the performance requirements demanded by the next generation of studies. The optimized device utilizes Bowden cable actuation, high-performance materials, lateral support structures, and specific component geometry to meet these requirements. Furthermore, the design and manufacturing sections of this thesis, particularly, contain information which may usefully inform future optimization efforts. Finally, the section on future work further supports those efforts by detailing potential sources of optimization for the next generation of ankle exoskeleton devices.

Chapter 2 Literature Review

The following section summarizes design approaches, results, benefits, and drawbacks of leading exoskeleton devices. The information learned in this review informed the design and manufacture of the optimized exoskeleton device presented in this thesis.

2.1 Sawicki Passive Exoskeleton

The Sawicki device is an unpowered ankle exoskeleton which utilizes a clutch actuated spring positioned in parallel with the Achilles tendon of the user [21]. It provides supplemental ankle torque by using a custom designed clutch to engage the spring at 10% of the stride cycle and disengage at 60% of the stride cycle. After disengaging, the ankle is free to rotate during the swing phase of the gait. The average supplemental ankle torque provided by this design was approximately within the range of $.075\text{-}.125 \text{ Nm} \cdot \text{kg}^{-1}$ and reduced the net metabolic cost of walking by $7.2 \pm 2.6\%$ in healthy subjects [21] [20].



Figure 1: Sawicki Passive Device (profile view) [20]



Figure 2: Sawicki Passive Device (rear view) [20]

Key features of the mechanical design are the bilateral carbon fiber support struts, footplate, shank interface, spring lever arm and clutch. The user interfacing parts were custom made for each participant using carbon fiber laid up on plaster molds. The extensive use of carbon fiber provides sufficient strength to deliver torque reaction forces while contributing to the minimal weight of the device (407g, Size 8 US). Additionally, the custom molding ensures optimal mating of user-device interfaces to reduce discomfort and improve force transmission to the shank. The results show that this passive device can achieve similar levels of assistance as powered devices by storing energy early in the gait cycle and releasing it throughout toe off.

However, the device has notable disadvantages. The spring lever arm attached to the heel of the device required for converting spring force into ankle torque protrudes several inches posterior to the heel. This extended feature may impair ergonomics in down-stair or negative hill walking. The bilateral support struts and footplate structure also protrude significantly in the lateral directions. This may further reduce walking ergonomics as the ankles pass each other during swing phase. Additionally, this device must be set for a steady, predetermined walking speed and is unable to automatically adjust to variable gait, limiting the practical functionality [21].

This device requires significant user dorsiflexion in order to load the spring and provide ankle assistance. Consequently, it would be unsuitable for those with conditions such as crouch gait which alters dorsiflexion gait patterns [22]. Finally, the assistive torque is limited by the passive nature of the device. While spring stiffness directly correlated with assistive torque, the stiffest springs tested resulted in higher metabolic demand than the no-exoskeleton and no-spring conditions [20]. If this result is caused by increased muscular demand during the loading phase,

then the potential to achieve further reductions in metabolic demand through passive devices of this nature is likely limited.

2.2 Harvard Exosuit

The Harvard Exosuit is an untethered, wearable robotic device designed as a tool for improving gait normalization in poststroke walking [9],[23],[17]. Key features of its mechanical design include a waist-mounted actuator assembly, Bowden cable force transmission, fabric calf wrap, and cable-interfacing insole. The device provides gait assistance by creating torque at the waist in the actuation assembly and transmitting it to the ankle through Bowden cable. This Bowden cable is terminated in a fabric wrap located at the calf. The steel wire within the Bowden cable then continues unshielded to the foot, where it connects to insole straps posterior and anterior of the ankle joint. Gait phase and ankle moment feedback are obtained using an ankle mounted inertial measurement unit and integrated load cells in the calf wrap, respectively. This feedback ensures that assistance is synchronized to gait pattern and that prescribed torques are achieved. Studies conducted using this device have shown increased forward propulsion and ground clearance in patients with stroke associated impairment but no reduction in walking energy cost [24].

The powered actuation of this design provides the user with gait assistance even in the presence of impaired dorsiflexion, making this device useful for a wider range of populations than its passive counterparts. Additionally, the utilization of Bowden cables allows the majority of the device weight to be situated at the hips, reducing the burden of distally located mass. The calf wrap is low profile and could possibly be worn under clothes. Finally, insole attachment points

located directly anterior and posterior of the ankle joint have the potential to reduce undesirable rotation of the calf wrap by minimizing the moment about the shank.

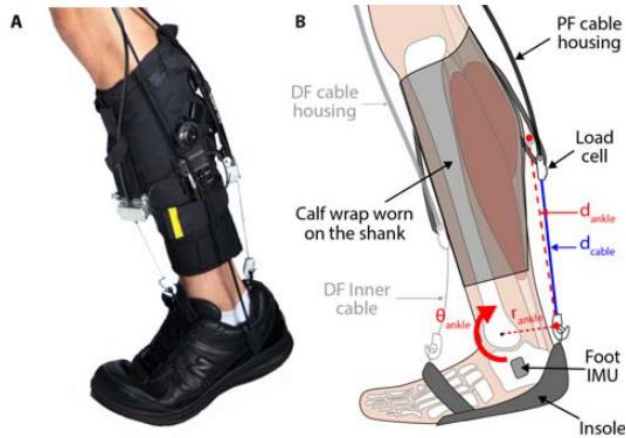


Figure 3: Exosuit Shank Interface [17]



Figure 4: Exosuit [17]

Drawbacks of this design include its relatively substantial weight, 2:1 motor to leg ratio, friction supported shank interface, and a limited plantarflexion moment arm. The device weight of 3.8 kg per leg of assistance is likely too heavy to be practically used outside of clinical settings, largely negating any benefit of wearing the device under clothing. This high mass may have been responsible for the finding that the device did not reduce walking energy demand, despite the increased efficiency associated with improved gait patterns. The use of separate motors dedicated to dorsiflexion and plantarflexion may be a significant contributor to this increased weight. The calf wrap relies on friction to ensure that the Bowden cables do not push the wrap down the shank when the distance between the ankle and hip decreases as in walking or sitting. For this reason, precise Bowden cable sizing is also vital. An insole attachment point directly posterior of the ankle joint limits the ability to practically increase the length of the moment arm

generating plantarflexion torque. By using this attachment point location, any increase to this moment arm will protrude directly posterior to the heel, possibly reducing downhill and down-stair walking ergonomics at greater moment arm lengths. Limiting the length of this moment arm requires any necessary changes in gear ratio be addressed in the motor assembly.

2.3 Collins Tethered Exoskeleton

The Collins exoskeletons are tethered end effectors designed to deliver a wide range of plantarflexion torque profiles to the ankle joint [15]. Alpha and Beta designs were created to emphasize high lateral compliance and reduced envelope, respectively. The designs each feature Bowden cable force transmission, bilateral carbon fiber support frames, series elastic elements at the heel, extended heel moment arms, fabric calf cuffs, and ground interfaces located beneath the toe. Force from an offboard motor is transferred through the Bowden cable and provides plantarflexion torque by actuating the heel moment arm of the device. Plantarflexion force is then transferred to the ground through the toe plate and torque reaction force is generated at the shank by the fabric calf cuff. A series elastic actuator is located at the heel to improve torque control. Load cells and strain gauges are utilized by the Alpha and Beta models, respectively, to provide torque feedback. The devices weigh .835 kg and .875 kg and have a range of motion of 30 degrees of plantarflexion and 20 degrees of dorsiflexion. Results showed peak torques of 120 Nm and 150 Nm and RMS errors of .751 Nm and .125 Nm, respectively, for the Alpha and Beta designs.

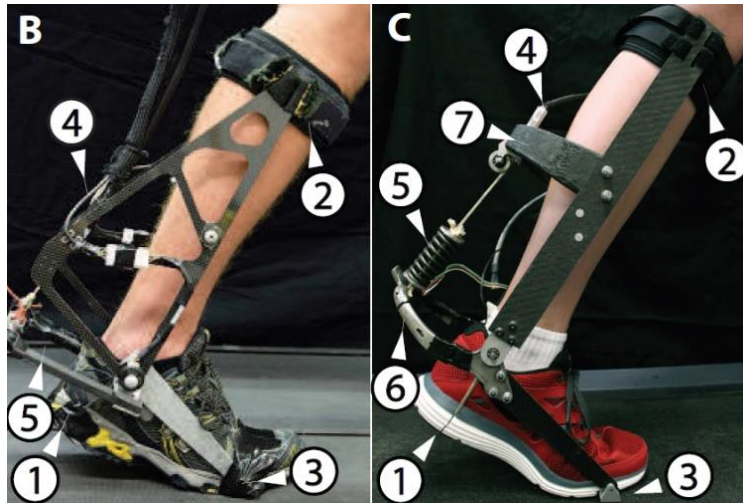


Figure 5: (B): alpha design (C): beta design [15]

The design features of these devices provide several advantages for performance and ergonomics. The use of carbon fiber components coupled with the bilateral support frame allows these designs to achieve very high assistance torques while being relatively light weight. The strain gauges utilized in the beta design naturally incorporate torque sensing into existing features rather than using a dedicated torque sensor. Directional compliance of frame components gives the user a natural range of inversion and eversion while walking. Finally, the adjustability of the calf cuff and frame components allow these devices to fit a wide range of users.

These devices are not without their disadvantages. The light weight of these devices largely derives from their tethered nature. Were these of a more practical, untethered design, it is likely that the lightweight and high torque capacity features would be significantly reduced. The medial protrusion of the bilateral supports was noted to cause increased step width and occasion collision in users, reducing metabolic efficiency and ergonomics [15]. The configuration of the

ground interface leads to the frame relying on friction at the calf cuff to support its weight rather than being self-supporting during a zero-torque condition. Additionally, the configuration of the ground interface requires structural modification of the user's shoe to produce a level walking surface. The titanium heel lever arm featured in the Beta design was produced through electron sintering, a costly additive manufacturing process, and protrudes significantly posterior to the heel, potentially reducing walking ergonomics in variable terrain. Finally, the design has no capacity to produce dorsiflexion assistance and little opportunity for modification to accommodate this feature.

2.4 Herr Ankle Exoskeleton

This device is an untethered ankle exoskeleton designed to provide plantarflexion assistance torque with the goal of reducing the metabolic cost of loaded walking. The primary design features are a shank mounted motor and transmission assembly, waist-mounted battery and motor controller assembly, and fiberglass struts located at the lower leg. Gait phase is determined using a pressure sensitive insole and optical encoder in the initial design and an IMU in a later configuration. Starting at 43% of the gait cycle, plantarflexion assistance torque is generated when the motor assembly tightens the cord that is connected to the fiberglass struts. These struts create a moment about the ankle, transferring plantarflexion force through the forefoot of the boot. As the actuator reaches .2 radians of plantarflexion, a zero-torque condition is applied, permitting unrestricted dorsiflexion. Testing of the initial design showed a loaded walking metabolic improvement of $8 \pm 3\%$ when compared to the no-exoskeleton condition [8]. An optimized design later showed an unloaded walking improvement of $10 \pm 3\%$ [25].



Figure 6: Initial Herr Device [8]



Figure 7: Optimized Herr Device [25]

Benefits of the mechanical design of this device include the ability to achieve high levels of assistance torque and a straightforward strut design. Transmission ratios of 120:1 and 160:1 for the initial and optimized designs, respectively, in concert with a robust strut configuration, resulted in the generation of 120 Nm of ankle torque assistance. This is similar to values achieved in tethered designs and an order of magnitude greater than the passive Sawicki device [15][21]. The bilateral strut design ensures that reaction forces generated at the shank are uniformly

applied, minimizing risk of shank interface rotation. Additionally, the strut configuration requires minimal fabrication effort and has a minimally intrusive interface with the foot of the user.

Disadvantages of this design center on lack of performance potential and ergonomic issues. The initial and optimized designs weigh 4.0 kg (2.3kg on lower legs and 1.7kg on waist) and 3.6 kg (2.12 kg on lower legs and 1.48 kg on waist), respectively. The significant distal mass negatively affects metabolic performance and limits performance potential unless relocated closer to the center of mass of the user. Additionally, this device has no potential to produce dorsiflexion assistance without significant design changes, eliminating a potential source of further metabolic improvement. The particularly distal location of the of the shank interface in the optimized design results in large reaction forces when compared to an interface location closer to the knee. These increased shank forces may be uncomfortable to the user at high assistance torques. The struts in the initial design protrude significantly in the posterior and medial directions, increasing the likelihood of inadvertent collisions and increased step width. Finally, the strut-shoe interface may not be practical in recreational shoes and requires shoe modification.

2.5 Original Lerner Exoskeleton

This device is a powered, untethered exoskeleton designed to reduce the metabolic cost of walking in children and young adults with cerebral palsy through the application of ankle assistance torque. The primary features of this device are a waist mounted motor and motor controller assembly, Bowden cable force transmission, lateral aluminum struts, aluminum insole, thermoplastic shank interface, and an aluminum pulley concentric and lateral to the ankle joint. Gait phase is determined using Force-Sensitive-Resistors located on the aluminum insole and

torque feedback is achieved using a torque sensor located at the ankle joint. Ankle assistance torque is provided when motor torque is transferred through Bowden cable to a pulley located at the ankle. Torque reaction forces are generated at the shank interface and aluminum insole. Larger and Smaller assemblies were made to fit a range of users, with masses of 2.20 kg and 1.85 kg, respectively. Results from initial testing of five participants with cerebral palsy showed a $19 \pm 5\%$ improvement in the metabolic cost of walking compared to the no-exoskeleton condition [7].

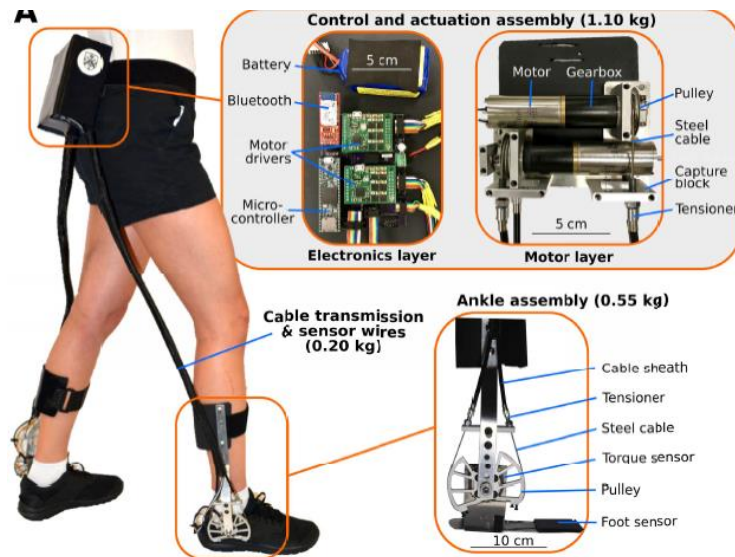


Figure 8: Original Lerner Exoskeleton [7]

The design of this device has several advantages when compared to similar exoskeletons. The powered actuation provides gait assistance even in users with reduced dorsiflexion range of motion, broadening the potential user base compared to passive devices. The configuration of the ankle assembly allows this device to provide dorsiflexion as well as plantarflexion assistance, further increasing the potential user base to include people in need of dorsiflexion assistance. The waist mounted motor and control assembly, Bowden cable actuation system, and minimalist

ankle assembly contribute to the device's minimal weight and allow the majority of the device mass to be situated near the center of mass of the user. These features strongly correlate with increased metabolic performance [26],[27]. The lack of medial ankle structure eliminates the risk of medial collision events and device-associated increased step width during walking. The location of the ankle pulley leads to minimal device protrusion posterior to the ankle joint. This results in minimal impairment to ergonomics in negative slope or down stair walking and gives the potential for significant gear ratio modifications at the ankle. Finally, the foot interface is compatible with a wide range of lightweight shoes.

Disadvantages of this device's design are primarily focused on execution rather than fundamental approach. The lateral shank supports and insoles are made from aluminum, which has less strength and rigidity than the carbon fiber used in comparable components of other exoskeletons [21][15]. These attributes lead to increased device weight and shank interface rotation as well as reduced durability. The shank interface is made from a flexible thermoplastic that readily deforms under load, decreasing torque transmission efficiency and contributing to uncomfortable interface rotation. Flexibility of the lateral supports, narrow ankle pulley channels, and angular play of the ankle thrust bearings all contribute to a high incidence of the steel cable slipping out of the ankle pulley grooves. When this occurs, the cable in the motor assembly can become contorted and further use of the device is impossible until the steel cable is realigned both on the ankle pulley and within the motor assembly. The varying departure angle of the steel cable from the motor spool and the narrow diameter of the tensioner creates a sawing effect on the steel cable at the Bowden cable entry point, reducing the durability of the steel cabling. The use of a motor spool also leads to significant maintenance time and effort when

replacing steel cabling as the motor box must be disassembled and the steel cable properly wound. The torque sensors located at the ankle are relatively heavy and high-profile, contributing to increased distal mass and increased calf interface rotation, respectively. Finally, the steel cabling is anchored to the ankle pulleys using set screws which are insufficient for high torque applications and prone to stripping.

Chapter 3 System Level Design Criteria

Establishment of system level design criteria is necessary to ensure that design of components and assemblies support high level goals. Accordingly, the following section details system level design criteria, their importance, and associated performance goals.

3.1 Device Mass

Added mass significantly increases the metabolic cost of walking, particularly when this mass is distally located [28]. One study found that the net metabolic cost of walking increased by approximately $7.6W$ (+3.28%) for every additional kilogram of mass added to a user's backpack [2].

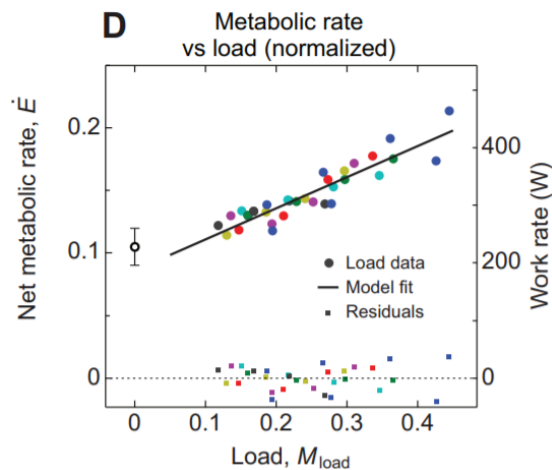


Figure 9: Net Metabolic Rate vs Load [29]

The effect is more prominent in children as added mass represents a greater proportion of bodyweight than in adults. For example, the youngest and lightest participant in an exoskeleton study by Lerner et al. had a net metabolic reduction of only 4% compared to the study average

of 19%. The authors attributed this to the high mass of the device relative to the user's mass (11.8% of bodyweight) [7]. For these reasons, minimizing device mass is a primary goal in exoskeleton design. The Harvard Exosuit excels at minimizing distal device weight, with a lower leg mass of just 502g per leg [17]. However, the total device mass of 3.8kg per leg is much heavier than exoskeletons with similar performance [7][20]. A design goal of approximately 500g per leg distally located and 2.5kg total would likely be achievable and support high metabolic reductions.

3.2 Ergonomics

Device ergonomics refers to the comfort of the device and the degree to which it interferes with user activity. A design which is comfortable encourages use of the device and ensures that users will be able to wear it for long enough periods of time to experience benefits. Interface migration is a significant source of discomfort and inefficient force transmission [18]. This occurs when device interfaces move relative to the user during walking. This movement causes friction and subsequent irritation of soft tissues [18]. Improper interface design can also cause discomfort when interface migration is minimized by unduly compressing soft tissue [19].

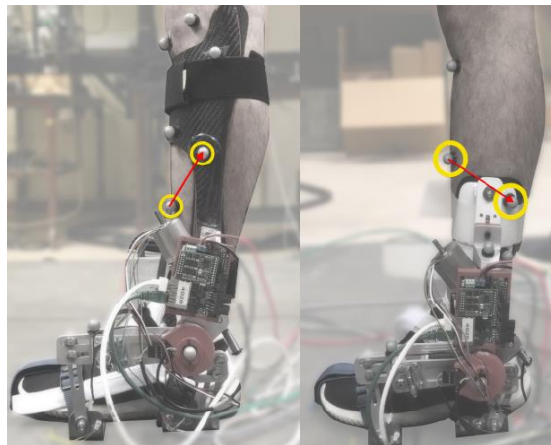


Figure 10: A short shank interface (right) creates larger torque reaction forces and greater soft tissue compression [18]

Minimal device interference supports reduced terrain restrictions and minimizes metabolic inefficiencies associated with altered gait patterns. Significant medial device protrusion has been shown to increase step width and limb collisions, the former of which is associated with increased metabolic cost of walking [30],[31]. Significant device protrusion posterior to the ankle joint as seen in the Sawicki passive exoskeleton may impair user gait when walking downstairs or on decline surfaces [20].



Figure 11: Passive Exoskeleton with significant Posterior Protrusion [32]

An optimized ergonomic design should minimize interface rotation, exoskeleton associated increases in step width, terrain restrictions, and user discomfort.

3.3 Durability

Durability in this context refers to the amount of time that the exoskeleton can function without requiring repair or maintenance. An exoskeleton which is highly durable will be more practical in settings without ready access to maintenance services such as in some clinical settings. Accordingly, durability goals can be informed by exoskeleton usage in clinical studies. A clinical

rehabilitation study by Conner et al. utilized resistive exoskeleton training for a total of approximately 100 minutes over 4-5 sessions, while an assistive study by Lerner et. al showed an average of 130 minutes of training per participant [10],[7]. As these walk times occurred over multiple visits, a goal of 60 minutes of exoskeleton walk time without need for repair is likely to satisfy clinical needs.

3.4 Torque Tracking

Torque tracking is a measure of how well an exoskeleton device achieves a prescribed torque profile. It is a primary performance metric, as an inability to consistently meet prescribed torques can result in reduced performance through poorly timed torque application and insufficient peak torques [33]. Root-mean-square-error is the primary tool used to quantify torque tracking in many exoskeleton studies [8],[15],[7]. Lerner et al. achieved a high level of metabolic performance with a trial root-mean-square-error of $0.042 \pm 0.004 \text{ Nm} \cdot \text{kg}^{-1}$. This value represents a desirable minimum value to ensure that an optimized mechanical design will achieve satisfactory torque tracking-associated metabolic performance.

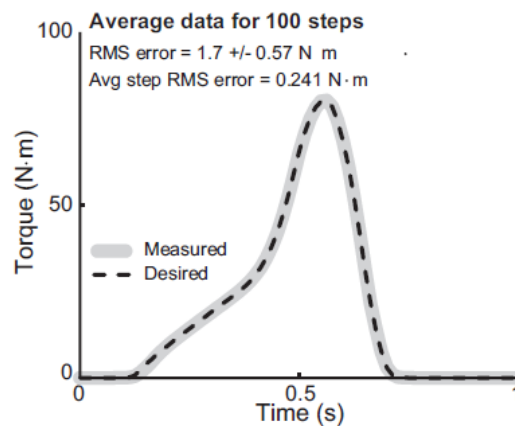


Figure 12: Torque Tracking, Measure and Desired vs Time [15]

It has been shown that there is a direct correlation between exoskeleton assistive torque and metabolic cost of walking [30]. This finding and the potential to assist heavier adults provide motivation to ensure that an optimized mechanical design will allow for the application of high levels of assistive torque. Orekhov et al and Lerner et al. achieved significant metabolic reductions with upper assistive torque values of approximately of $0.30\text{Nm} \cdot \text{kg}^{-1}$ [34], [7]. Utilizing this value for an adult user with a mass of 80kg gives a target maximum assistive torque value of approximately 25Nm.

Chapter 4 Design Concepts

While system level design criteria are outlined in section 3, the following sub-sections will detail design at the sub-assembly and component level. This includes fundamental function, specific goals and limitations considerations, the design features which served those considerations, the final optimized design, and any noteworthy designs which were considered or pursued but ultimately not included in the final design.

4.1 System Overview

The optimized ankle exoskeleton device presented in this thesis is based on the device created by Lerner et al. [7]. This device is examined in detail in section 2.5 of this thesis, but the function and benefits of this platform will be summarized here briefly. The device functions by providing ankle joint torque using a Bowden cable actuated ankle pulley. This torque is generated and prescribed by a motor and controller assembly located at the waist. Joint torque reaction forces are generated with a shank mounted cuff and a footplate located within the user's shoe.

This platform has high potential for optimization because it is untethered, locates a large proportion of device mass near user center of mass, has lateral support and actuation structures, and utilizes a practical device-shoe interface. Untethered devices are practical for clinical applications and can be used for over-ground walking, while tethered devices are typically limited to treadmill walking. Lateral support structures ensure that users experience minimal gait alteration from protruding medial structures. The lateral ankle pulley location allows for gear ratio modification at the ankle without significantly increasing device protrusion posterior to the

ankle joint. Finally, the footplates utilized in this platform allow for dorsiflexion as well as plantarflexion assistance and are compatible with a wide range of lightweight footwear. The device presented in this thesis optimizes component design and material selection but maintains the fundamental design approach of the original Lerner exoskeleton.



Figure 13: Original Lerner Exoskeleton [7]



Figure 14: Optimized Exoskeleton

4.2 Footplate

The device-shoe interface is the component of an exoskeleton system responsible for generating and directing distal ankle torque reaction forces. This interface is configured as a footplate in the original Lerner exoskeleton and the device presented in this thesis.



Figure 15: Original Lerner Footplate [7]



Figure 16: Optimized Footplate

For plantarflexion assistance, reaction forces are directed toward the ground during the propulsive phase of gait, assisting in forward propulsion. For dorsiflexion assistance, reaction forces are directed up toward the sole of the foot, assisting the user in achieving ground clearance during the swing phase of gait. For plantarflexion resistance, as used in the gait rehabilitation study by Conner et al, reaction forces are directed up toward the sole of the foot during the propulsive phase of gait, providing a training stimulus [10].

Footplate design must support and account for several goals and limitations. These can be described by the following criteria: strength, stiffness, durability, weight, and ergonomics.

The footplate must be strong and durable to ensure that high torque values can be consistently achieved, while minimizing mass to reduce metabolic burden. Mass of the footplate is particularly important, as its distal location is the most metabolically impactful of all the exoskeleton components [28]. Accordingly, carbon fiber was chosen to replace the aluminum used in the original Lerner exoskeleton, due to its high strength to weight ratio, durability, and ability to form complex geometries [35]. Furthermore, half of the carbon fiber layers that make up the laminate

have a 0/90 fiber orientation, ensuring a high degree of strength in the sagittal and coronal planes. In addition to material considerations, a gradual shoulder geometry was utilized in the transition from the ankle to the sole portion of the footplate to ensure reduced stress concentrations compared to those present in the steep shoulder of the original Lerner footplate.

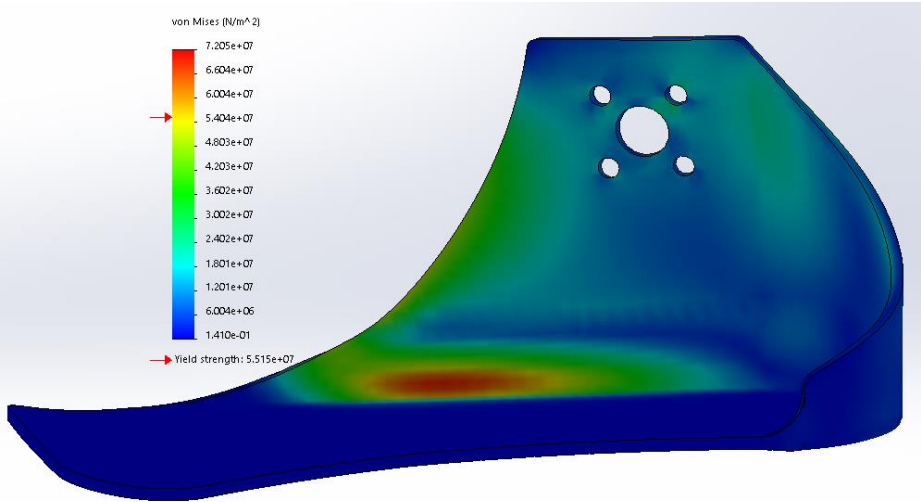


Figure 17: stress in shoulder, Optimized footplate

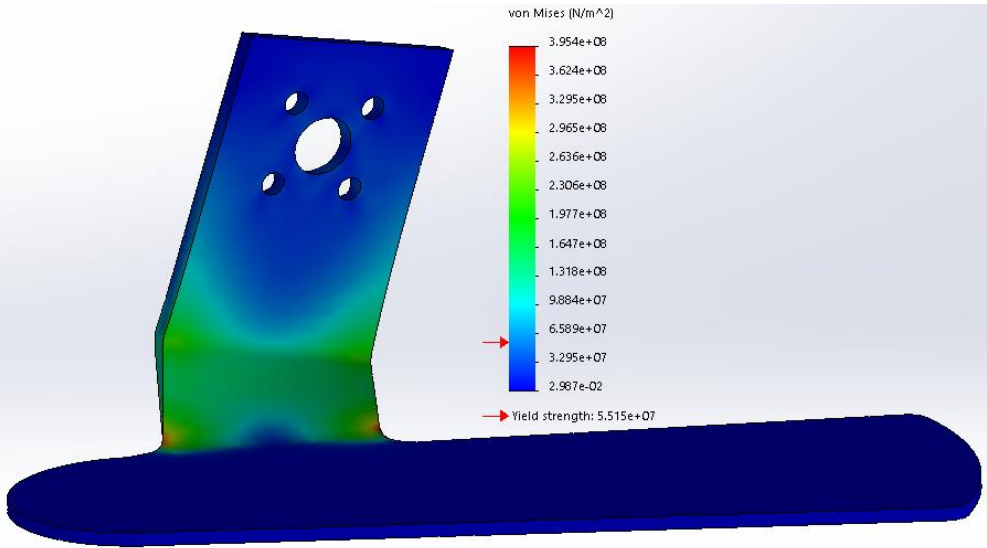


Figure 18: stress in shoulder, Original Lerner footplate

A high degree of rotational stiffness in the ankle portion of the footplate is an important feature to reduce rotation of the shank interface about the leg. This is because the lack of medial support structure in this design results in a moment being generated about the leg when torque reaction forces are produced at the shank interface.

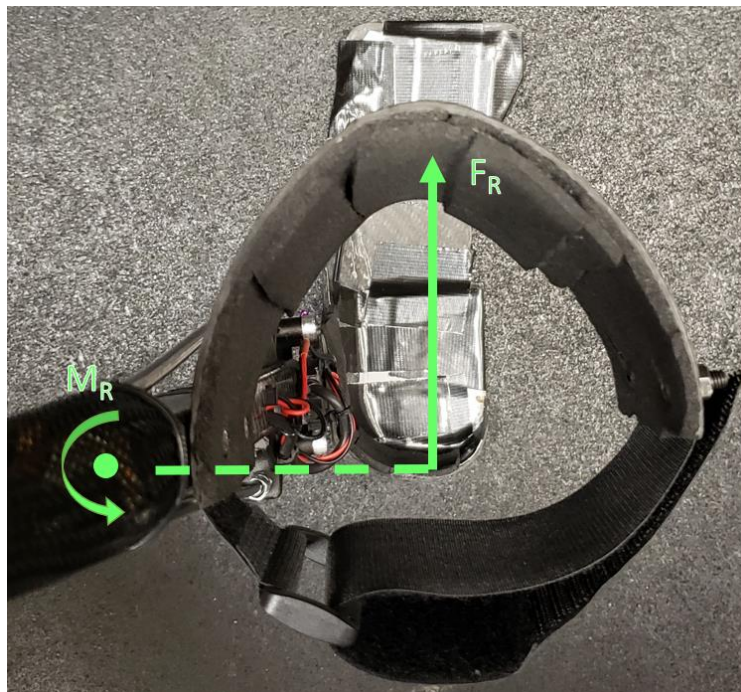


Figure 19: lateral support moment

Interface rotation is not only uncomfortable but may cause delayed torque reactions and a subsequent reduction in torque tracking accuracy. To address this need, the footplate incorporates specific geometric and material features. A heel cup geometry and a 45/45 fiber orientation in half of the layers of the laminate work in concert to increase the rotational rigidity of the ankle portion of the footplate by improving the moment of inertia and shear modulus of the optimized footplate, respectively, compared to the original Lerner footplate.

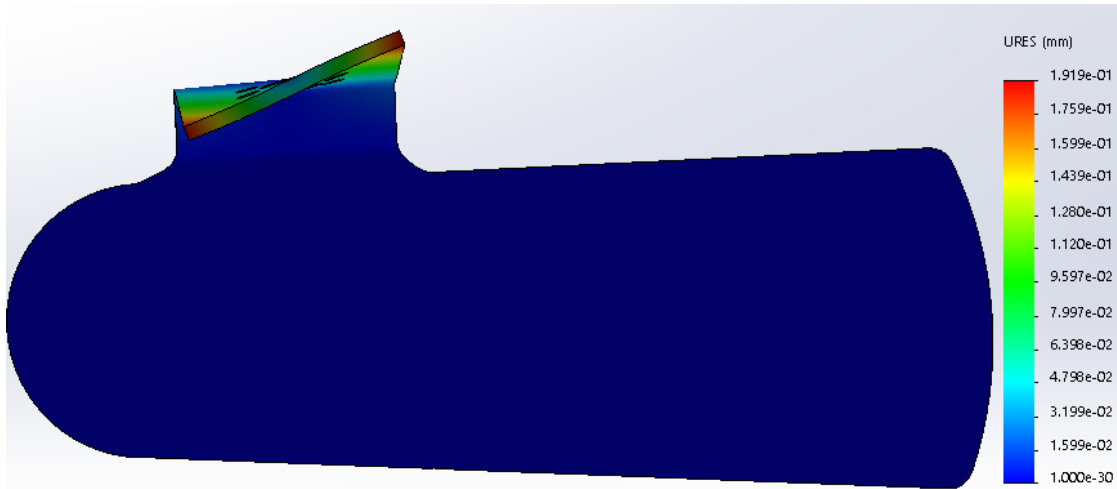


Figure 20: rotational deflection, Original Lerner footplate

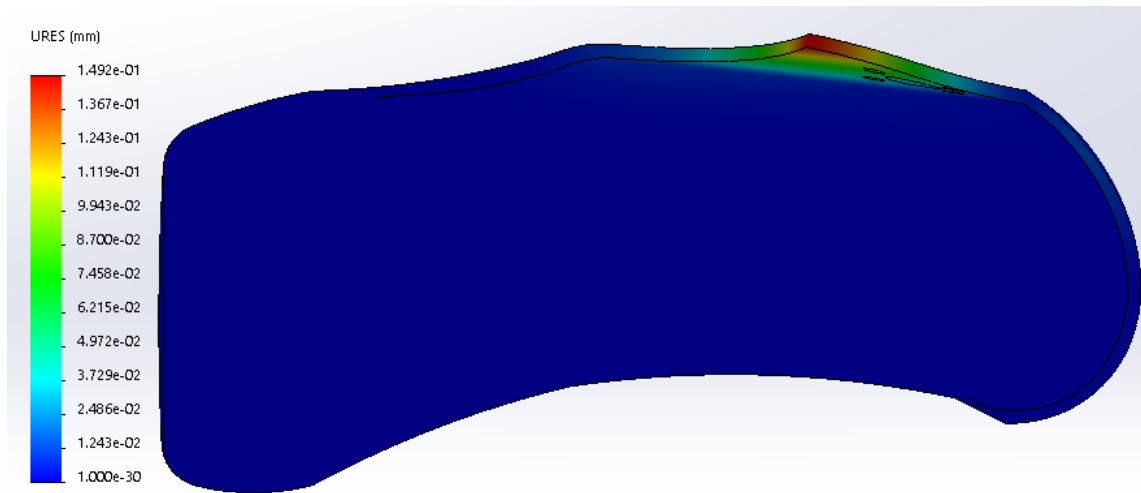


Figure 21: rotational deflection, Optimized footplate

A high degree of bending stiffness between the ankle and sole portions of the footplate is also important to ensure that assistive torque stays in-plane with user plantarflexion. The heel cup geometry and 0/90 oriented carbon fibers layers support this requirement. The heel cup acts as a support structure for frontal plane bending, while the 0/90 layers improve stiffness by ensuring that frontal plane bending loads act primarily along the carbon fiber strands rather than the much weaker and more flexible matrix material.

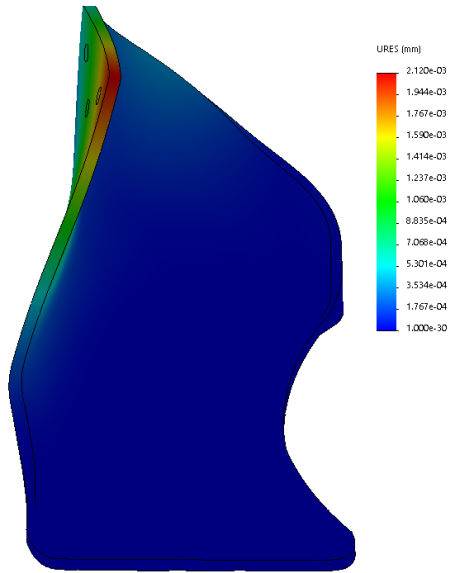


Figure 22: frontal plane deflection, Optimized footplate

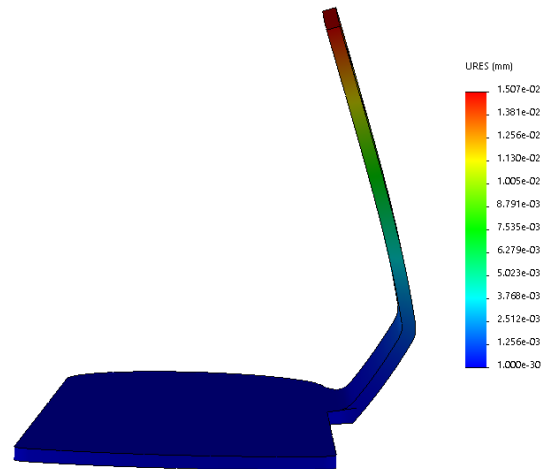


Figure 23: frontal plane deflection, Original Lerner footplate

Remaining specific goals of the footplate include the ability to support the mass of the lower leg assembly, minimal negative impact on gait patterns, and the ability to fit comfortably in a wide range of lightweight shoes.

A footplate which is incapable of supporting the mass of the lower leg assembly will likely create a condition where the lower leg assembly is either supported by the tension of precisely sized Bowden cable or by friction of the shank interface. Neither circumstance is optimal. The former will reduce the functional size range of the exoskeletons and lead to inconsistent lower leg assembly support as the direct distance spanned by the Bowden cable varies throughout the gait cycle. The latter may result in users increasing tightening of shank interface strapping, leading to increased soft tissue compression and associated discomfort. The footplate design presented here provides this support by transferring lower leg assembly mass directly to the user's shoe

and minimizing any undesirable moments generated about the forefoot by footplate-ground reaction forces.

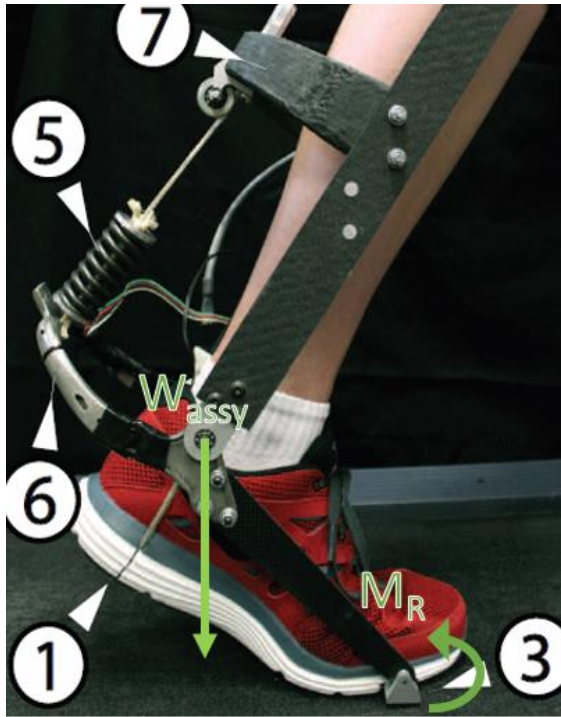


Figure 24: moment generation about forefoot [15]



Figure 25: self-supporting Optimized assembly

Minimal gait interference is an important consideration in footplate design because the metabolic benefits provided by the exoskeleton could be diminished by footplate-associated increases in step width and because limb collisions could negatively impact user experience [31]. The optimized footplate attempts to minimize these outcomes by eliminating protruding medial features. Footplate geometry can also negatively impact gait patterns through a heel-drop phenomenon. This phenomenon occurs when a combination of footplate length, shape, and stiffness result in the user's heel pulling away from the shoe and footplate during the final

moments of the propulsive phase of gait, when the angle between the toes and forefoot becomes acute. This phenomenon is uncomfortable and may create an additional muscular burden on the lower leg of the exoskeleton user.

The footplate design presented in this thesis addresses this issue by using a curved forefoot geometry and an optimized length. The curved forefoot geometry allows the footplate to rock forward during toe-off, mirroring the angle change of the user's foot.



Figure 26: curved forefoot geometry during propulsive gait phase

Heel drop minimization can also be achieved by limiting the amount that the footplate extends beneath the metatarsals, an approach apparently used in the Sawicki Device [21]. However, this approach may result in the device center of pressure moving posterior to the user's biological center of pressure during plantarflexion, reducing the degree to which the device accurately reflects the user's gait.

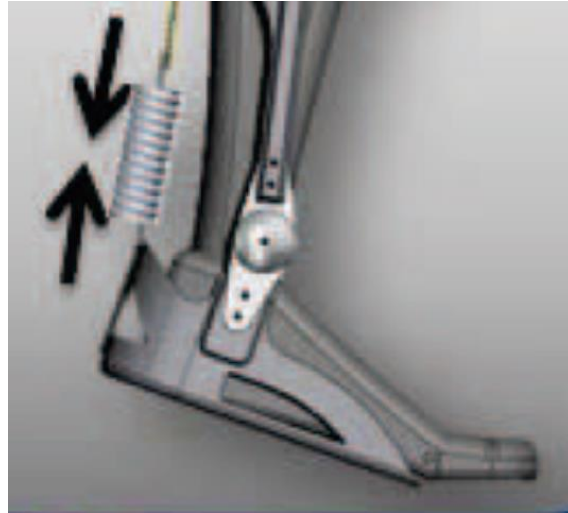


Figure 27: short footplate design [21]

Forefoot curvature addresses the heel drop phenomenon while minimizing possible center of pressure migration. However, extreme forefoot curvatures were found to be uncomfortable in initial prototyping. Consequently, finalized forefoot curvature and length were determined through an iterative prototyping process.

Finally, a driving consideration in the design of an optimized footplate is the need for compatibility with a wide range of lightweight footwear. The footplate must be compatible with lightweight footwear because distal mass has a significant impact on the metabolic burden of the user [28]. A device which is only compatible with heavy footwear such as the Herr device may have reduced performance potential [8].



Figure 28: high distal mass device [8]

Additionally, a footplate which is compatible with a wide range of shoes has an increased potential for use in non-research settings and decouples use of the exoskeleton device with the availability of a potentially narrow range of footwear. The footplate presented in this thesis supports these considerations by utilizing a component geometry which is compatible with the interior envelope of a typical athletic shoe and by declining to rely on the structure of the footwear to provide torque reaction forces.

Approaches to the design of an optimized footplate which were also pursued but ultimately found to be non-ideal for our system include footplates produced through fiberglass-reinforced additive manufacturing and a forefoot-strut design similar to the Collin's emulator [15].



Figure 29: fiber-reinforced 3D printed footplate



Figure 30: strut design foot interface

The former had an inferior strength to weight ratio compared to its carbon fiber laminate equivalent and was found to be less comfortable due to its relative thickness. Additionally, initial testing showed poor torque tracking at plantarflexion torque values greater than 20 Nm, as well as noticeable footplate deflection. These may have been a result of the reduced stiffness of the Onyx and fiberglass materials used in this footplate compared to the carbon fiber laminate of the optimized design. While initial findings indicate that this design approach is sub-optimal for high torque applications, they do suggest the potential for low torque applications such as in children-specific devices and devices for users who only require dorsiflexion assistance. The primary advantage of this approach is the minimal manufacturing effort.

The attempted strut approach was pursued due to its potential for low mass, but was ultimately found to be sub-optimal due to the difficulty in attaching the interface to the user's shoe, its inability to support the mass of the lower leg assembly during swing phase, and a noticeable discomfort resulting from the extruded surface the component creates beneath the forefoot portion of the user's shoe. The attachment and discomfort issues may have been solvable by creating modifications to the user's footwear, but initial testing showed that this design's inability

to support the mass of the lower leg assembly during swing phase was a significant problem, as it created migration of the lower leg assembly down the user's leg.

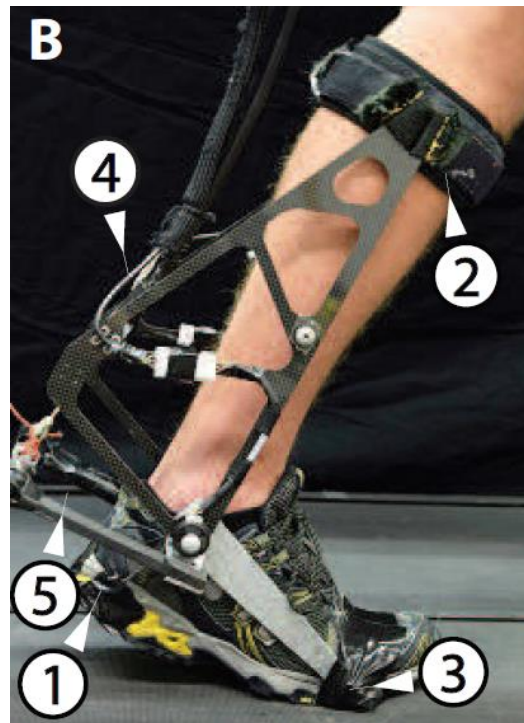


Figure 31: non-self-supporting device [15]

4.3 Lower Leg Assembly

The role of the lower leg assembling in an ankle exoskeleton is to provide ankle joint torque and generate reaction forces to that torque by interfacing with the shank of the user. Both the original Lerner lower leg assembly and the optimized assembly presented in this thesis accomplish this utilizing lateral support structures and Bowden cable actuated ankle pulleys. It should be noted that the custom torque sensor, ankle pulley, and inline pulley configuration presented in this section were designed and fabricated by Ph.D. student Greg Orekhov. Intermediate ankle pulley

(Figure 41) and Bowden cable bracket designs were created by the author and included features which are present in the final designs such as wide pulley channels, wire termination crimping sleeves, and 3D printed fabrication. However, the final designs presented here were found to be more optimal due to the utilization of an inline rather than cantilevered pulley location.

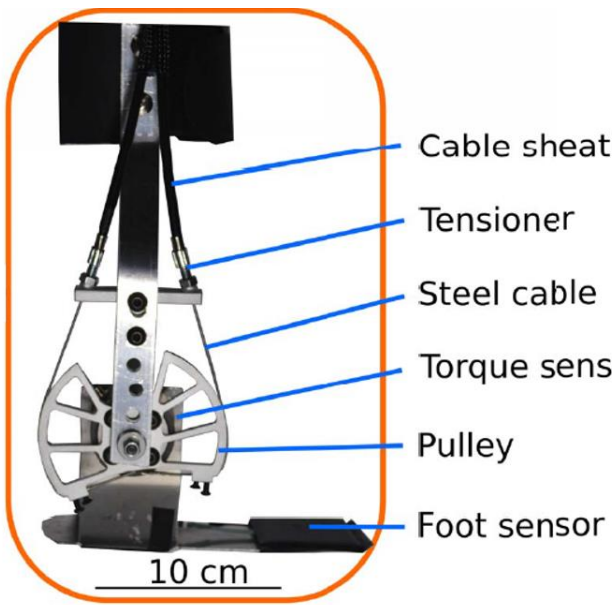


Figure 32: Original Lerner lower leg assembly [7]



Figure 33: Optimized lower leg assembly

To satisfy the requirements of our system, the optimized lower leg assembly needs to be strong, stiff, durable, light, ergonomic, reliability, and capable of both plantarflexion and dorsiflexion torque generation.

The assembly must have the strength and durability to consistently generate high torques. This ensures that the exoskeleton can be used for high assistance torque studies and adult populations. Due to the distal location of this assembly, it must accomplish these goals without

sacrificing a lightweight construction. Additionally, the assembly components should prioritize sagittal plane stiffness to minimize flexibility-associated errors in torque tracking.

The optimized design presented in this thesis supports these goals by utilizing high strength, lightweight, carbon fiber components, and a custom ankle torque sensor. The carbon fiber materials used in the optimized assembly are significantly lighter, stiffer, and stronger than the aluminum used in the original Lerner assembly [35]. Additionally, the custom torque weighs just 20 grams, making it significantly lighter than the 73-gram commercial sensor used in the original Lerner assembly [7].

Lower leg assembly design must ensure minimal negative impact to ergonomics to minimize risk of reductions in metabolic performance and positive user experience [30],[31]. The lower leg assembly presented in this thesis supports this aim by utilizing lateral support structures and an ankle pulley location that is lateral and concentric with the ankle joint. The use of lateral support structures eliminates protruding medial features, reducing the potential for exoskeleton-associated increases in step width and limb collisions. The location of the pulley allows for significant gear ratio modifications at the ankle without creating significant device protrusion posterior to the ankle joint, an outcome which has the potential to restrict down-stair walking.

Comfort is prioritized in this design to support positive user experience and the prospect of study participants being able to complete full durations of prescribed testing protocols. The lower leg assembly presented here supports this goal by utilizing features to optimize application of torque reaction forces at the shank and reduce interface rotation about the lower leg.

The length of the lateral carbon fiber tube used in this assembly was selected to minimize torque reaction forces. By extending this feature up the length of the shank, the torque reaction forces at the shank interface are reduced compared to a configuration which utilizes shorter supports.

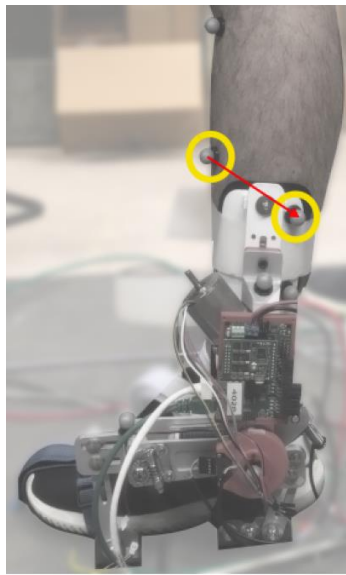


Figure 34: device with short shank interface supports [18]

Additionally, the geometry of the shank interface was designed to reflect the shank of a typical user to support a consistent force distribution. Furthermore, initial prototyping has shown the potential benefit of a more straightforward donning process with the anterior shank interface configuration compared to the posterior shank interface used in the original Lerner assembly [7].

Interface rotation can have a significant negative impact on comfort [18]. The lower leg assembly presented in this thesis addresses this issue through the design of the shank interface, carbon fiber support tube, torque sensor, and bearing configuration.

The shank interface is made of carbon fiber layered in a 0/90 fiber orientation to increase sagittal plane stiffness. The intent of this configuration is to minimize the migration of the interface center of pressure away from the tibial axis, supporting minimal moment generation. The Original Lerner assembly, in contrast, utilized a flexible thermoplastic material in its shank interface [7]. The carbon fiber support tube has a high shear modulus and moment of inertia, supporting reduced interface rotation through minimization of angular deflection of the lateral supports [36]. The custom torque sensor has a low coronal plane profile, reducing the length of the moment arm responsible for generating rotation of the shank interface about the lower leg. This dimension is 5.35 mm in the custom torque sensor while the same dimension is 25.4 mm in the original Lerner configuration [7].



Figure 35: moment arm, COTS torque sensor, cantilevered design [34]

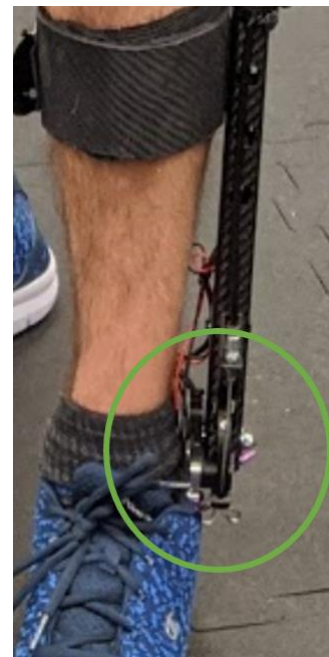


Figure 36: moment arm, Optimized exoskeleton

Finally, the bearing configuration utilizes two flanged ball bearings mounted in the support tube to allow free rotation of the ankle joint while minimizing bearing-associated shank interface rotation. The concentricity of the bearings restricts angular deviation resulting from tolerances within the bearings. The use of adapting interfaces in this configuration allows for high preload bolt torques to be achieved without negatively affecting bearing performance, minimizing interface rotation resulting from insufficient bolt torque.

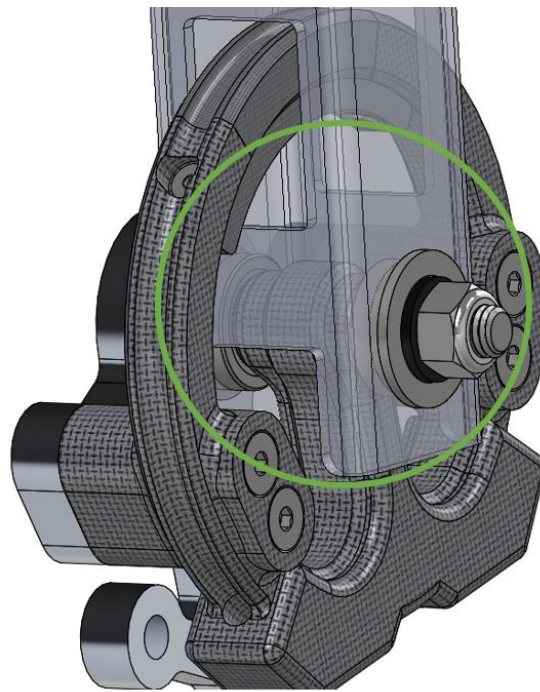


Figure 37: bearing configuration, Optimized exoskeleton

Reliability in the optimized lower leg assembly is supported by features which minimize the occurrence of wire-pulley misalignment and by the utilization of crimping sleeves to terminate that wire. Wire misalignment occurs when the steel wire actuating the ankle pulley migrates out of the pulley channels, causing the exoskeleton to cease functioning until the wire can be

realigned. Additionally, this results in temporary loss of tension, which can negatively affect components of the motor assembly.

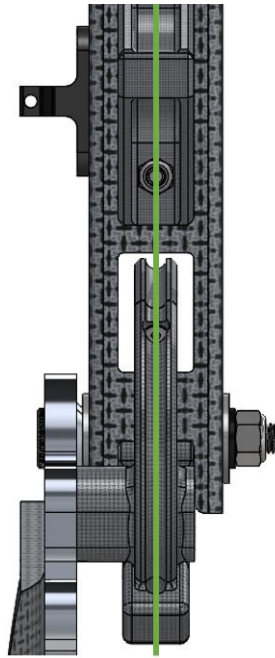


Figure 38: Bowden cable and ankle pulley alignment, Optimized exoskeleton

This issue is addressed in the optimized assembly by features of the carbon fiber support tube, ankle pulley, and bearing configuration. The carbon fiber support tubes have a high degree of stiffness in the coronal plane, ensuring that bending loads experienced by this component do not cause misalignment between the Bowden cable termination brackets and the ankle pulley channels. Additionally, the ankle pulley was designed with wide channels to mitigate wire misalignment risk in the case of support tube deflection or lack of pulley-bracket collinearity resulting from imprecise fabrication or assembly. The features of the bearing configuration which support minimization of shank interface rotation also support wire misalignment minimization.

These features minimize angular deviation allowed by the bearings, which can result in ankle pulley rotation in the coronal plane and subsequent impact to wire-pulley alignment.

The optimized lower leg assembly utilizes crimping sleeves to terminate the steel wire at the ankle pulley. Initial prototyping has found these to have a greater holding capacity than the set screws used in the original Lerner assembly [7]. Additionally, they are compatible with the 3D printed ankle pulley used in the optimized design. Finally, reliability issues associated with thread stripping are eliminated.

Dorsiflexion torque capability allows an exoskeleton to be useful to a wider range of people than a device which is only capable of providing plantarflexion torque [20],[25]. An exoskeleton device with this capability can be used in resistance studies and has a high potential to benefit those in need of dorsiflexion assistance [37]. This feature is supported in the optimized lower leg assembly using a symmetric ankle pulley, which can provide dorsiflexion torque when actuated in the counterclockwise direction.

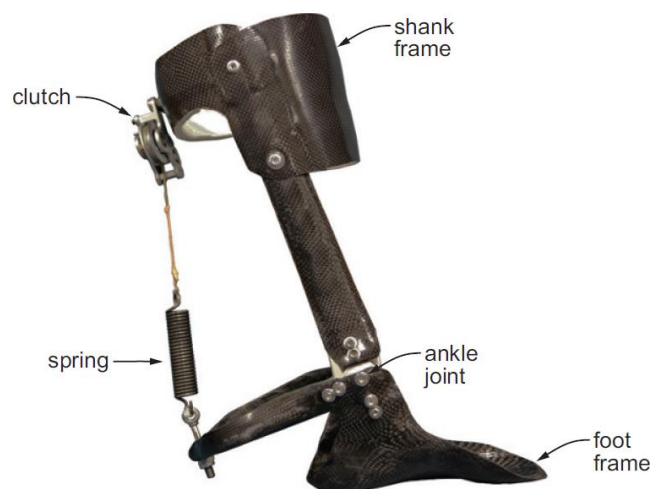


Figure 39: plantarflexion-only device [20]

While there were no lower leg assembly design approaches which were pursued but ultimately not included in the final design, intermediate configurations did exist which shared several features of the optimized design but lacked others.

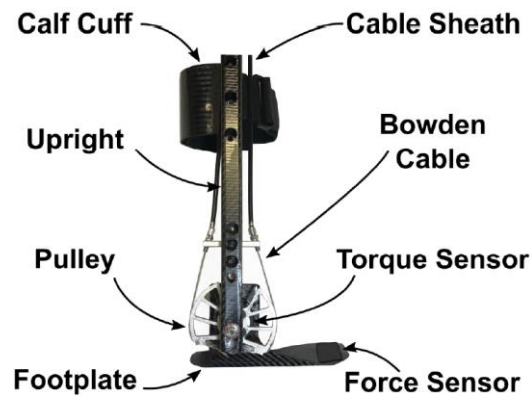


Figure 40: an intermediate lower leg configuration



Figure 41: intermediate design, 3D printed Pulley

Intermediate configurations utilized a support tube, carbon fiber components, a 3D printed ankle pulley, and an optimized bearing configuration but lacked a custom torque sensor and optimized

designs for the pulley, shank interface, footplate, and Bowden cable bracket components. As a result of these differences, the intermediate design had greater distal mass, greater lateral protrusion, was less comfortable, and produced greater moments about the shank compared to the final optimized assembly.

4.4 Motor Assembly

The motor assembly houses the motors and motor controller needed to produce torque and control the exoskeleton, respectively. In the device presented in this thesis, the motor assembly utilizes two gear motors (EC-4pole, Maxon, 16900 rpm, 123:1 reduction) located at the user's waist, and transfers motor torque through Bowden cable to the lower leg assembly. By locating these motors at the waist, the majority of the exoskeleton mass is near the center of mass of the user, improving metabolic performance [28]. This approach contrasts with exoskeleton devices which utilize more distal motor locations [8],[25].

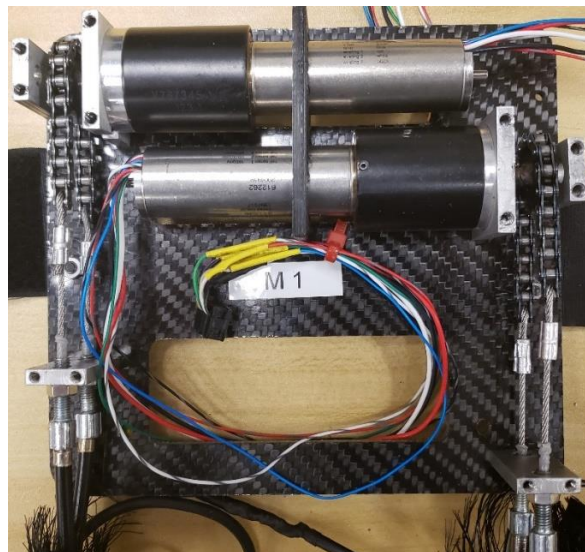


Figure 42: motor assembly (partially disassembled), Optimized exoskeleton

Motor assembly design must consider the following criteria: mass, durability, strength, stiffness, reliability, and serviceability.

Although the location of the motor assembly minimizes the metabolic burden associated with increased mass, this burden remains significant enough to warrant the inclusion of mass as a design criterion. This design criterion is supported in the optimized motor assembly by the use of lightweight, carbon fiber sandwich panels and a single motor per leg configuration. The sandwich panels have a higher strength to weight ratio compared to the aluminum used in the original Lerner motor assembly, reducing panel weight while providing the high panel strength and durability necessary to consistently achieve high torques [35]. They are also stiffer than aluminum, possibly reducing the likelihood of torque tracking errors stemming from panel flexibility. The motor configuration can provide both plantarflexion and dorsiflexion torque using a single motor per leg, halving the number of motors, and motor mass, compared to a configuration like that utilized in the Harvard Exosuit [17].

A primary source of durability issues in the original Lerner motor assembly is the wear incurred by the steel wiring as it moves back and forth through the tensioner located between the motor assembly and Bowden cable.

The optimized motor assembly presented in this thesis addresses this issue using a chain and sprocket torque transmission system and modified Bowden cable. The chain and sprocket transmission system ensures that the steel wire travels within a more consistent and narrower diameter as it enters and exits the tensioner. This contrasts with the spool transmission system used in the original Lerner motor assembly, which results in the steel wire traveling within a large

diameter due to a varying departure angle as the wire winds and unwinds from the spool. By maintaining a narrow envelope of travel, the chain and sprocket design minimizes contact forces between the wire and the tensioner, leading to decreased wear. Finally, motor noise in the chain and sprocket system should remain minimal due to the low sprocket speeds, which peak at approximately 135 rpm.

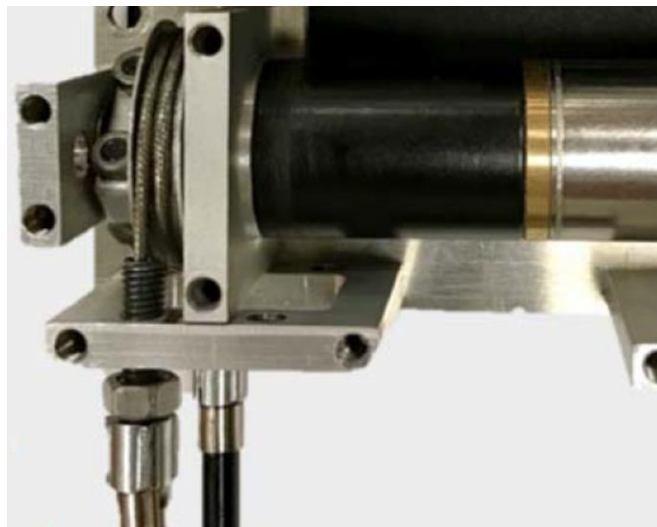


Figure 43: Spool and tensioner configuration, Original Lerner exoskeleton

The Bowden cable modification is accomplished by stripping the spiral steel housing away from the ends of the cable, leaving the interior plastic sleeving exposed. This sleeving is then threaded through the tensioner during assembly, where it protrudes and bends to accommodate angle deviations of the incoming steel wire, minimizing friction and wear.



Figure 44: stripped Bowden cable

Reliability of the motor assembly is important to ensure that the exoskeleton can operate without interruption for significant periods of time. This criterion stems from exoskeleton use in clinical studies, which have can have strict training protocols and limited capacity to address hardware issues during patient visits [10]. This is supported in the optimized motor assembly by the chain and sprocket torque transmission system.

Spool transmission systems like those utilized in the original Lerner exoskeleton and the Harvard Exosuit lead to tension generation in the steel wire wound about the motor spool [7],[17]. If wire tension is lost in another part of the system, this can result in rapid unfurling of the wire about the motor spool and a subsequent need to service the motor assembly for wire alignment. This rapid unfurling is unsurprising due to the minimal diameter of the spool compared to the wire, a ratio of approximately 20, while the recommended ratio for these diameters is 400. The chain and sprocket transmission system addresses this issue, as the chain in this configuration generates no reaction forces when configured about the motor sprocket. Subsequently, any loss

in tension which could result, for instance, from wire misalignment at the ankle pulley, will not guarantee motor assembly issues in this optimized configuration.

Finally, the chain and sprocket transmission system allows for replacement of the steel wire without disassembling the motor assembly and also allows for improved gear ratios compared to the motor spool design of the original Lerner assembly. The former feature may lead to reduced service times when changing exoskeleton sizing while the latter feature should allow for reduced ankle pulley diameters without sacrificing high ankle torque generation.

A design feature which was pursued but ultimately failed to be implemented in the final optimized motor assembly was the use of high strength braided fishing line (Dorisea Extreme Braid) rather than steel wire. This approach was attractive due to both the potential to eliminate issues with rapid unfurling at the motor spool during periods of tensions loss as well as minimization of bending stress incurred through winding about the motor spool. Unfortunately, this approach was found to be unsuitable due to minimal frictional wear resistance and difficulty terminating the line at the ankle pulley. However, the pursuit of this approach contributed to the design of the lower leg assembly, specifically the effort to reduce instances of wire misalignment at the ankle pulley.

Chapter 5 Validation

5.1 Validation Protocol

Validation was conducted at a system level to verify that the optimized exoskeleton device met performance goals. These goals are described by device mass, torque tracking, ergonomics, and durability.

Torque tracking, ergonomics, and durability were assessed from the results of a treadmill walk test. This test was conducted by having a subject walk at their preferred speed of 1.25 ms^{-1} while receiving iteratively increasing ankle torque assistance. Assistance torque ranged from 15 – 25 Nm, approximately $.21 - .35 \text{ Nm} \cdot \text{kg}^{-1}$. Assistance torque setpoints were maintained for a minimum of 10 gait cycles and in a variety of conditions. These conditions included the use of both open and closed loop control algorithms, high and low current motor drivers, and anterior and posterior shank interface configurations. Torque data was measured using a custom torque sensor located at the ankle. Ergonomics was quantified by recording the number of contralateral limb collisions during testing and soliciting subject feedback on device comfort after each walking trial. Additionally, shank interface relative motion data was collected with a Vicon motion capture system. Durability was determined by recording the number of instances in which the device required mechanical servicing within the approximately 1-hour testing period. Distal and total device mass were measured directly using a digital gram scale.

5.2 Device Mass

Mass of the Optimized Exoskeleton device sized for a 70.3 kg user with US size 10 shoe was found to be 385g grams per leg distally located and 2.07 kg total without battery. This results in approximately 37% of device mass being distally located. As shown in Figure 45 and Table 1, the distal and total mass of the optimized device presented in this thesis compares favorably with other leading untethered exoskeletons (battery mass not included for ready comparison). The Sawicki device has lower total mass than the optimized exoskeleton, but it should be noted that this design is passive, a design approach which leads to reduced mass, but more limited performance potential compared to powered devices. When considering just the powered devices, the Optimized exoskeleton is the lightest both distally and in total mass. It should also be noted that the Collin's tethered exoskeleton was not included in Figure 45 and Figure 47 as its tethered nature makes a total mass comparison with untethered device illogical.

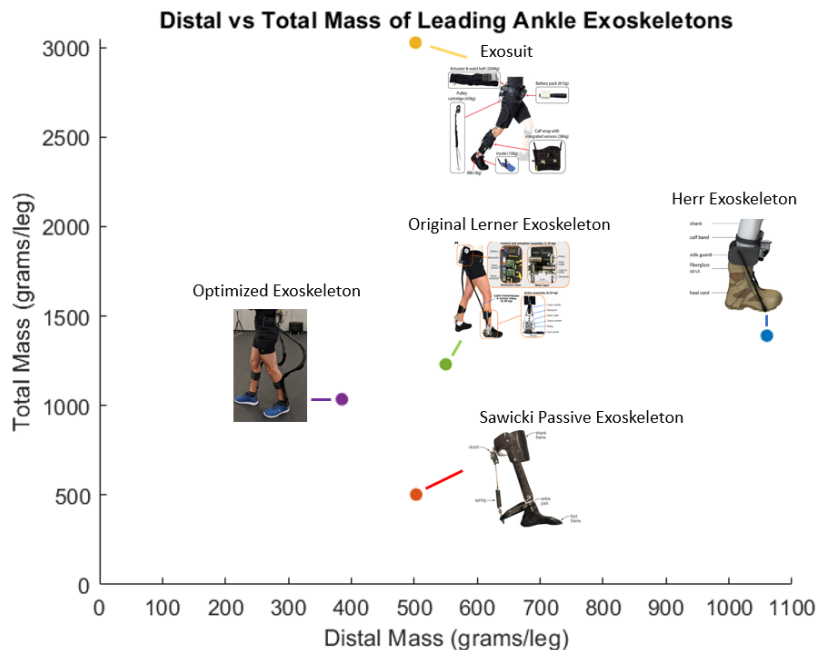


Figure 45: Distal vs Total Mass of Leading Ankle Exoskeletons

Table 1: Distal Mass, Total Mass, and Peak Plantarflexion Torque [7],[25],[20],[17]

	Distal Mass (grams/leg)	Total Mass (grams/leg)	Peak Plantarflexion Torque (Nm)
Original Lerner exoskeleton	550	1230	20
Herr exoskeleton	1060	1390	120
Sawicki Passive exoskeleton	503	503	30
Exosuit	502	3026	24
Collins Tethered exoskeleton	875	N/A	150
Optimized exoskeleton	385	1035	25

Figure 46, Figure 47, and Table 1 show that the optimized exoskeleton device presented in this thesis achieves similar levels of ankle assistive torque with minimal distal and total mass when compared to other leading untethered ankle exoskeleton devices.

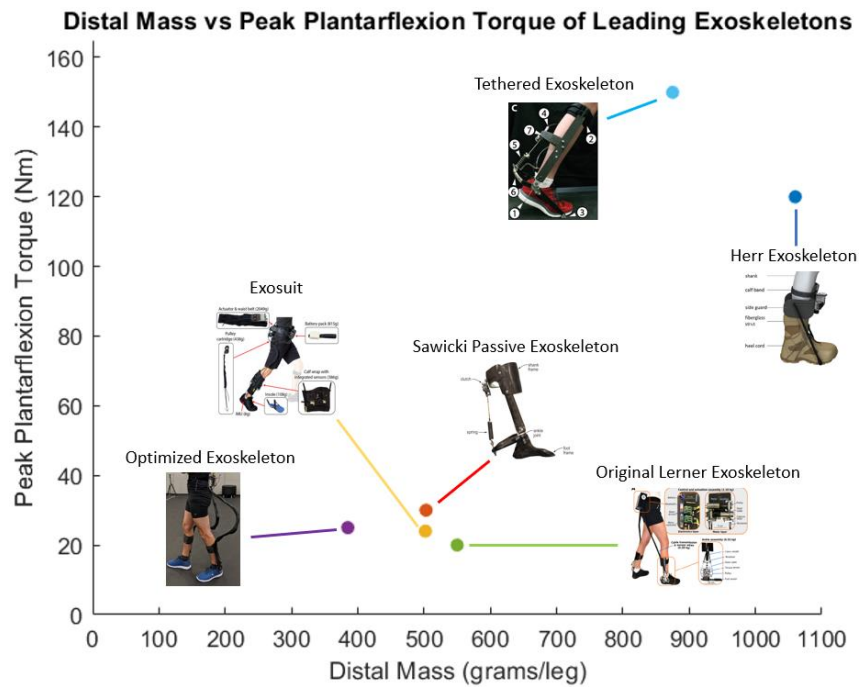


Figure 46: Distal Mass vs Peak Plantarflexion Torque of Leading Exoskeletons

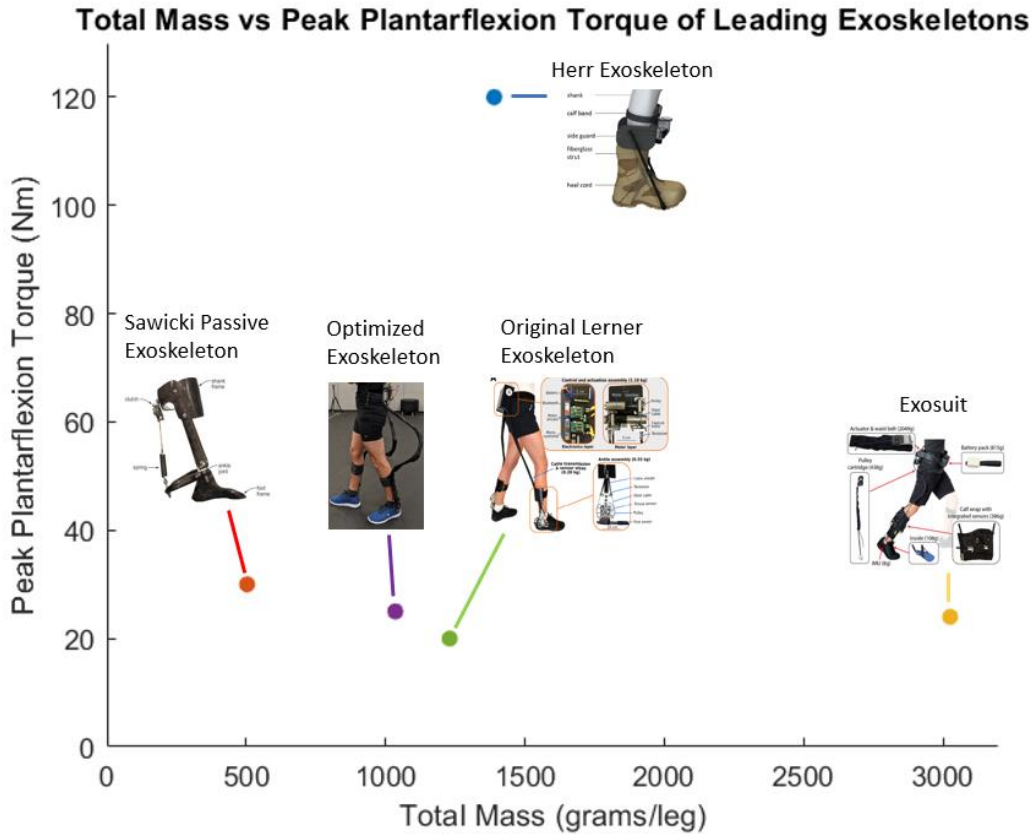


Figure 47: Total Mass vs Peak Plantarflexion torque of Leading Exoskeletons

Again, it should be noted that the Sawicki device a passive device. Additionally, while the Herr and Tethered exoskeletons are capable of high torque production, their practical applications are limited due to high distal mass and a tethered configuration, respectively [25].

5.3 Torque Tracking

Table 2 gives the average root-mean-square-error for each walking condition. From this data and Figure 49, several conclusions can be made. A positive correlation can be seen between assistive torque and RMSE values. The closed loop (CL) control algorithm condition was found to have reduced error rates compared to the open loop control algorithm condition, possibly due to the CL algorithm’s ability to adjust current supplied to the motors based on torque sensor feedback.

The CL algorithm condition at the 20 Nm setpoint resulted in an average RMSE value of 2.448 Nm, or $.035 \text{ Nm} \cdot \text{kg}^{-1}$ when normalized by user mass. The 15 Nm setpoint resulted in an average RMSE value of $.027 \text{ Nm} \cdot \text{kg}^{-1}$ when normalized by mass. These results represent approximately a 17% and 40% reduction in RMSE, respectively, compared to the $.042 \text{ Nm} \cdot \text{kg}^{-1}$ average error achieved by the original Lerner exoskeleton (Figure 50). Additionally, the 20 Nm setpoint at which this RMSE value was obtained with the optimized exoskeleton is the maximum torque value that the original Lerner exoskeleton can provide [7]. Finally, it was found that the posterior shank interface resulted in lower RMSE values than the anterior shank interface. This may be due to the lack of compressive foam on the posterior shank interface strapping, which supports minimal delay in force transmission at this interface. In general, the findings validate the design goal of providing accurate torque tracking over a range of assistive torque setpoints.

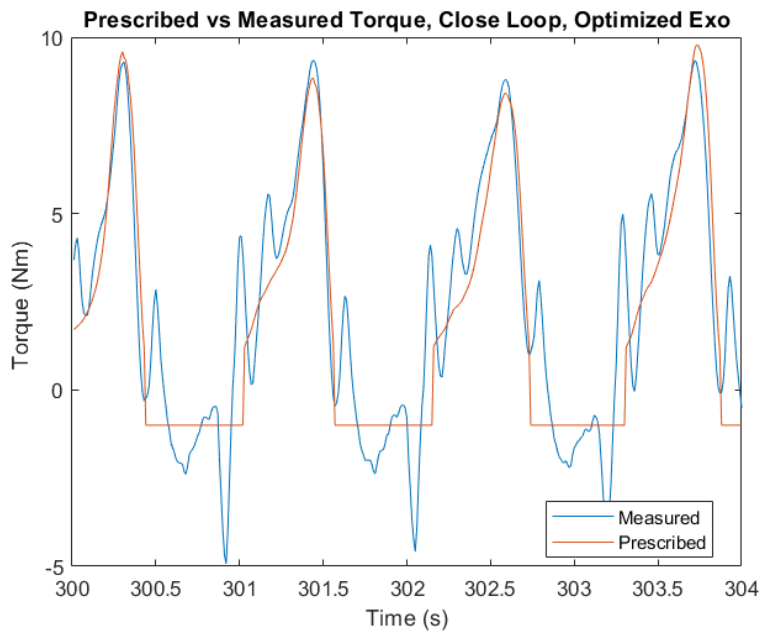


Figure 48: Prescribed vs Measured Torque, Close Loop, Optimized Exo

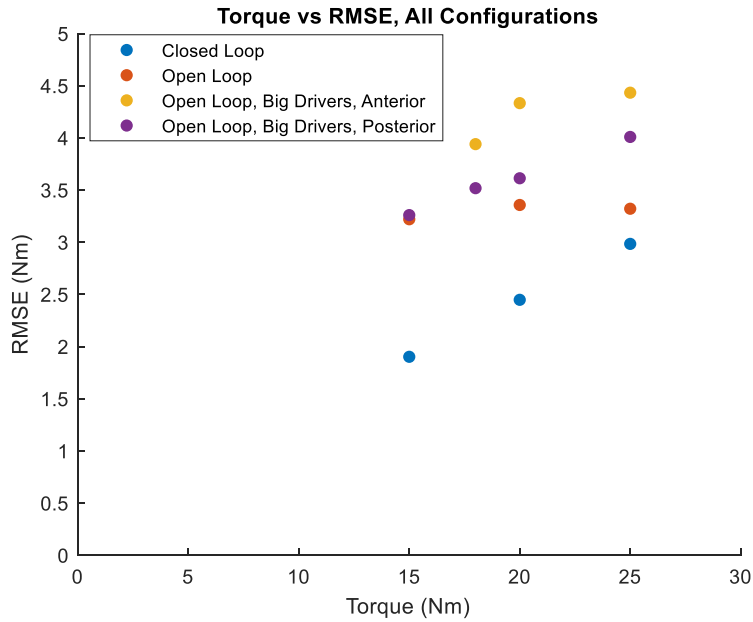


Figure 49: Torque vs RMSE, All Configurations

Table 2: RMSE, various walking conditions, Optimized device

Closed Loop Control Algorithm, small drivers, anterior shank interface		
Set Torque	RMSEAvg	RMSEAvg_Normalized_Mass
15	1.902	0.027
20	2.448	0.035
25	2.984	0.042
Open Loop Control Algorithm, small drivers, anterior shank interface		RMSEAvg_Normalized_Mass
Set Torque	RMSEAvg	
15	3.220	0.046
20	3.357	0.048
25	3.321	0.047
Open Loop Control Algorithm, big drivers, anterior shank interface		RMSEAvg_Normalized_Mass
Set Torque	RMSEAvg	
18	3.940	0.056
20	4.333	0.062
25	4.433	0.063
Open Loop Control Algorithm, big drivers, posterior shank interface		RMSEAvg_Normalized_Mass
Set Torque	RMSEAvg	
15	3.260	0.046
18	3.518	0.050
20	3.613	0.051
25	4.009	0.057

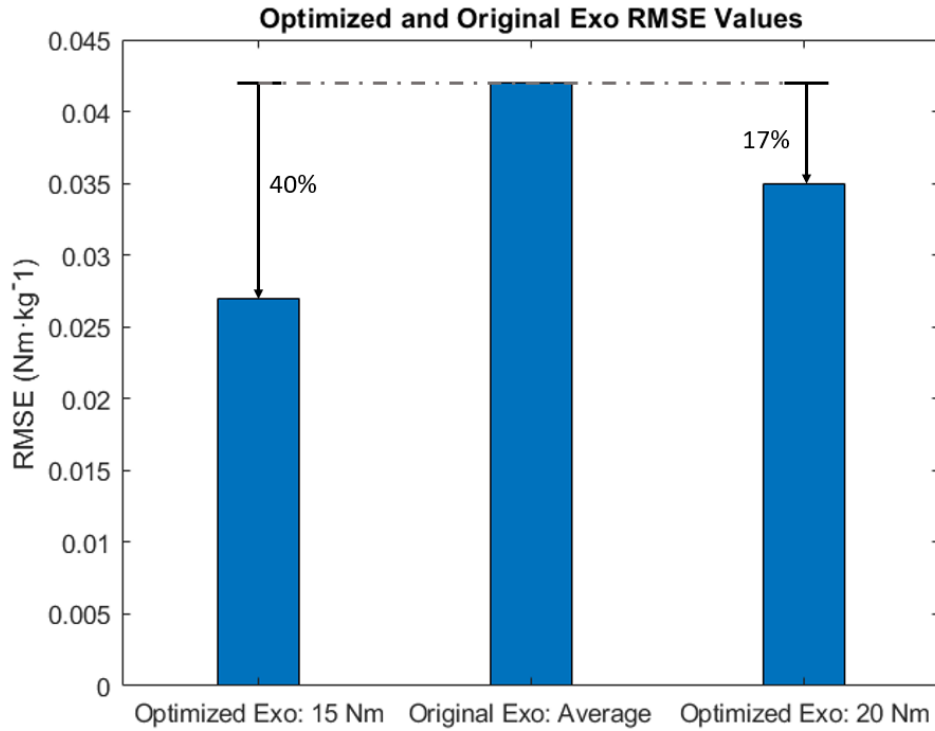


Figure 50: Optimized and Original Exo RMSE Values

5.4 Ergonomics

The testing protocol resulted in no contralateral limb collisions during the approximately 1-hr walk time. This was likely due to the lack of medial structure present in the design of the optimized device presented in this thesis. Additionally, the subject rated the anterior shank interface as being significantly more comfortable than the posterior shank interface, particularly at high torque set points and after extended walk times. This finding suggests that the reduced RMSE values seen with the unpadded posterior shank interface strapping may have come at the expense of decreased user comfort.

Figure 51 through Figure 54 show movement of the shank interface throughout the gait cycle, as well as the corresponding torque profiles (~ 20 Nm peak torques) for both the anterior and

posterior shank interface configurations. These show minimal movement of the shank interface relative to the user despite the relatively high assistance torque values. Figure 51 shows a shank interface tibial rotation range of just 9°, indicating that the material and design features of the lower leg assembly successfully minimized interface rotation. This is also supported by subject comfort feedback, which indicated minimal discomfort associated with interface movement. Additionally, the figures show minimal relative motion difference between the posterior and anterior shank interface configurations.

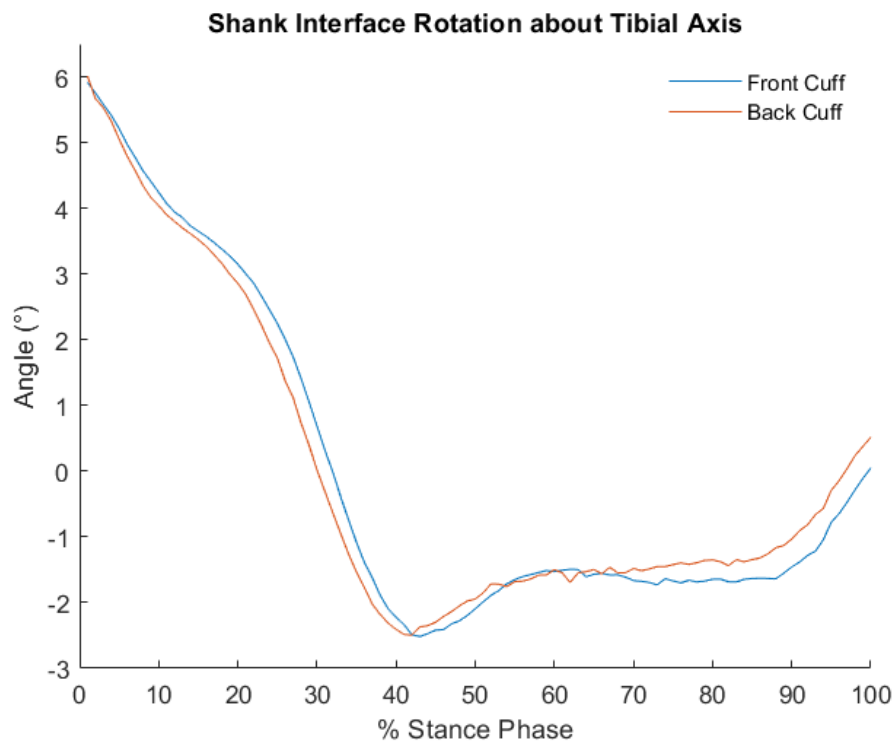


Figure 51: Shank Interface Rotation about Tibial Axis

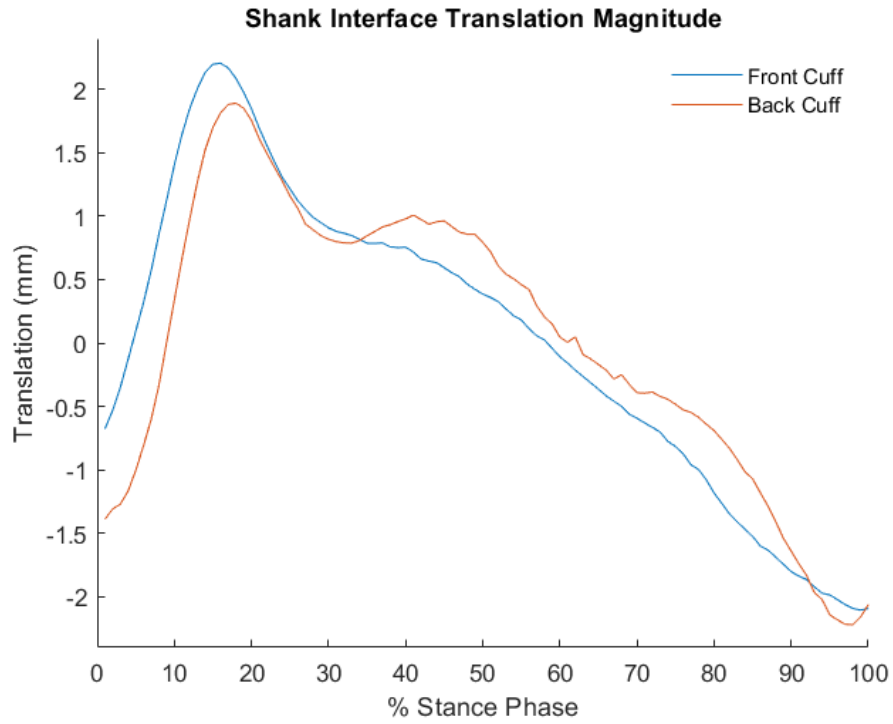


Figure 52: Shank Interface Translation Magnitude

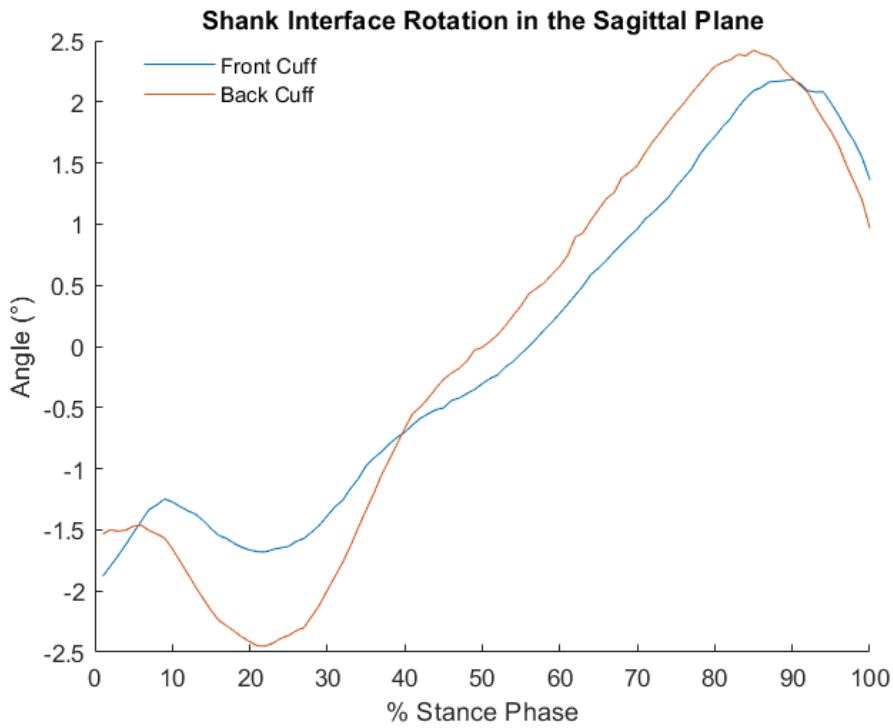


Figure 53: Shank Interface Rotation in the Sagittal Plane

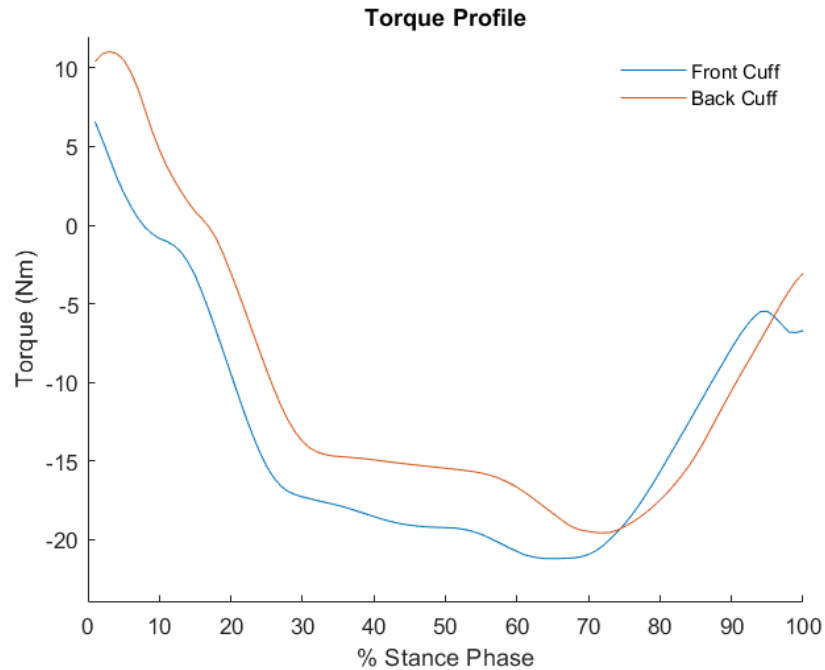


Figure 54: Torque Profile

Finally, the subject reported no instances of the “heel-drop” phenomenon described in section 4.2. These ergonomic findings show that the optimized exoskeleton device meets the ergonomic design goals of user comfort and unimpaired gait.

5.5 Durability

The optimized exoskeleton device presented in this thesis required no repairs during the approximately 1-hr walk time of the conducted testing. However, wire tension was adjusted between trials to ensure that torque actuation remained consistent. This need for tension adjustment was unexpected, and tension consistency issues should be addressed in future design optimizations. These findings indicate that the device is likely reliable enough to use in clinical studies, which typically utilize shorter walk times than the testing conducted for this thesis [7],[10],[17].

Chapter 6 Manufacturing

The components that make up the exoskeleton system presented in this thesis were variously fabricated using the following methods: additive manufacturing, out-of-autoclave carbon fiber layup, machining, and welding. Their manufacture utilized the following equipment: STEPCRAFT D-Series CNC, MarkForged Mark Two 3D printer, composite vacuum bagging supplies, RIDGID Wet Tile Saw, Dremel, and WEN Variable Speed Drill Press. This section will outline key aspects of the manufacturing process for components utilized in the exoskeleton system presented in this thesis.

6.1 Motor Assembly

6.1.1 Motor Panels

Motor panels were created utilizing a STEPCRAFT D-Series CNC to machine the panel perimeter and hole pattern out of a sheet of premade sandwich panel (Rockwest, Twill-Foam-Sandwich-Economy). The CNC produces a precise hole pattern, reducing risk of misalignment between brackets and supporting straightforward assembly. Hand files are then used to remove any sharp or protruding fibers created during machining.

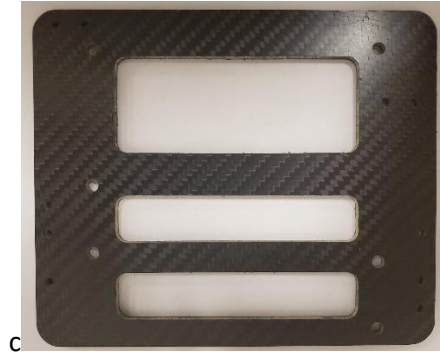


Figure 55: motor panel, Optimized exoskeleton

6.1.2 Chain and Sprocket

Manufacturing the chain and sprocket torque transmission system involves attaching a sprocket to the motor shaft and creating the chain-wire component which the sprocket interfaces with. Conventional machining is used to remove the sprocket hub in order to reduce weight and improve clearance. The sprocket is then welded to the motor shaft to ensure a strong and low-profile attachment. Finally, a handheld chain breaker is used to create chain of the desired length and steel wire is secured to the chain using wire crimping sleeves and a handheld crimping tool.

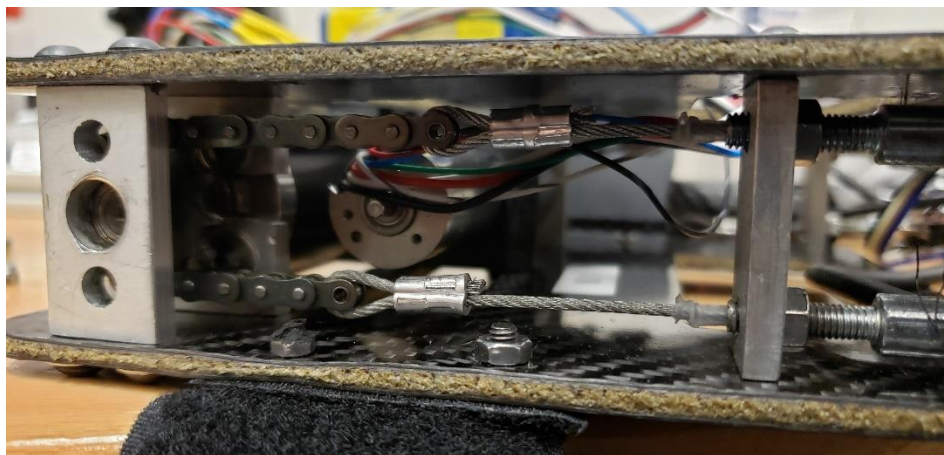


Figure 56: chain and sprocket transmission system, Optimized exoskeleton

6.2 Lower Leg Assembly

6.2.1 Footplate and Shank Interface Components

The footplate and shank interface components are made from bidirectional woven carbon fiber and manufactured using an out-of-autoclave curing process. This process utilizes a vacuum bagging technique to create pressure on the carbon fiber components during curing, supporting the removal of excess epoxy and the minimization of voids within the carbon fiber layers [38].

The first step in the manufacturing process is the creation of nesting component molds. These are interlocking molds which define the shape and surface finish of the carbon fiber parts. Each mold is made from the thermoplastic material Onyx and created using a MarkForged Mark Two printer. This additive manufacturing method provides inexpensive molds with accurate geometry, desirable surface finish, and minimal lead time. Additionally, the 3D printing process is straightforward, only requiring the upload of an .STL file and application of glue stick to the print bed.



Figure 57: interlocking 3D printed footplate molds



Figure 58: interlocking 3D printed shank interface molds

Mold release agents (Meguiar's Carnuba Plus Premium Paste Wax and Suave Extreme Hold Unscented Hairspray) are then applied to the molds to support straightforward mold removal after curing and minimal impact to component surface finish. Personal protective equipment used in the carbon fiber layup process include 3M half facepiece respirators with organic vapor/P100 cartridges, paint coveralls, sealing goggles, nitrile gloves, shop vacuum, and an air purifier.

Carbon fiber layers are cut from dry, bidirectional woven carbon fiber fabric (Rockwest, 2x2 Twill .012" thick) using fabric scissors and a template reflecting a projection of the mold surface. The shank interface is composed of eight 0/90 oriented layers, while the footplate uses four 0/90 layers and four 45/45 layers. After all the layers necessary for the layup have been cut, the matrix material (West Systems 105 Resin, West Systems 206 Slow Hardener) is then mixed and applied to a mold and each succeeding layer of carbon fiber. When each of the layers have been applied, the matching mold is placed on top and the mold-carbon fiber configuration is placed in a commercial-off-the-shelf (COTS) vacuum bag (Magicbag, original-medium). COTS vacuum bags are used for their consistent sealing.

The vacuum bag is then sealed, and the air removed, with special care being taken throughout this process to ensure that there is sufficient bagging material in any curved geometries of the mold. This minimizes the risk of a phenomenon known as bridging, where bagging material bridges over curved geometry rather than making complete contact with the mold, resulting in poor distribution of pressure and finish.

The components are then left to cure for a minimum of fifteen hours. The components are then removed from the bags, the molds are removed from the components, and machining can begin. A wet tile saw is initially used to remove the majority of excess material. A Dremel with a sanding tip is then used to achieve a more precise geometry and round edges. Finally, mounting holes are drilled using a drill press (WEN, Variable Speed - 4214) set to 3000 rpm with a carbide tipped bit. These bits are used due to their high durability and the significant wear inducing nature of carbon fiber machining [39].

6.2.2 Ankle Pulley and Bowden Cable Brackets

The ankle pulley and Bowden cable brackets are 3D printed using a Mark Forged Mark Two printer. Additive manufacturing with fiber reinforcement is useful for fabricating these components due to the ability to quickly create complex geometries that are light, strong, and relatively inexpensive. The process to print these parts is relatively straightforward. The .STL part files are first uploaded to Eiger.io, the website which manages the Markforged printer. The printing orientations of the ankle pulley and Bowden cable bracket are then specified to ensure that filament layers are properly oriented for component loading conditions.

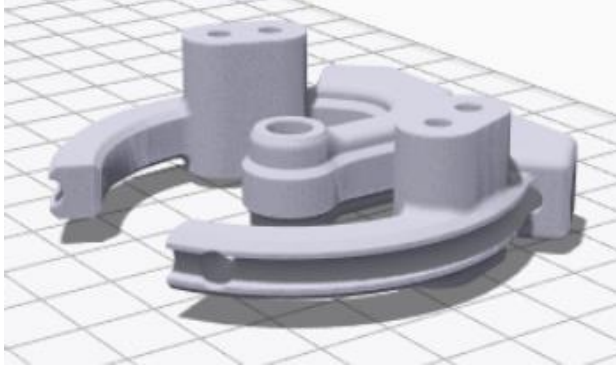


Figure 59: Eiger printing orientation, ankle pulley

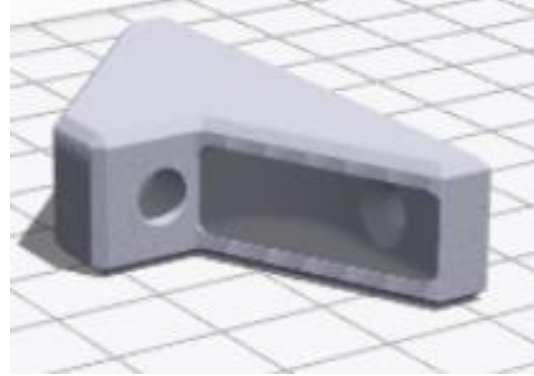


Figure 60: Eiger printing orientation, Bowden cable bracket

Within Eiger, carbon fiber reinforcement is selected from a drop-down menu and reinforcement fiber options are specified. Finally, glue stick is applied to the print bed and the print is initiated in Eiger.

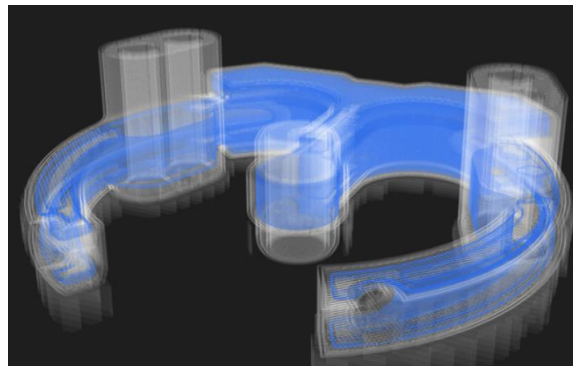


Figure 61: carbon fiber reinforcement specification, ankle pulley

6.2.3 Carbon Fiber Support Tube

The carbon fiber support tubes are machined using a RIGID Wet Tile Saw, D-Series STEPCRAFT CNC, and hand files. Lengths of tube are first cut using the wet tile saw. This saw minimizes carbon fiber generation and has features which support flush, level cuts. The STEPCRAFT is then used to create the hole pattern for attaching interfacing components. The STEPCRAFT is used for its

precision machining and water-bath feature. The former ensures that the ankle bearing holes of the support tube are sized appropriately for press fitting and reduces risk of ankle pulley and Bowden cable bracket alignment issues. The water-bath feature minimizes carbon fiber dust generation during machining. Finally, a hand file is used to remove any sharp or protruding features created during the machining process.

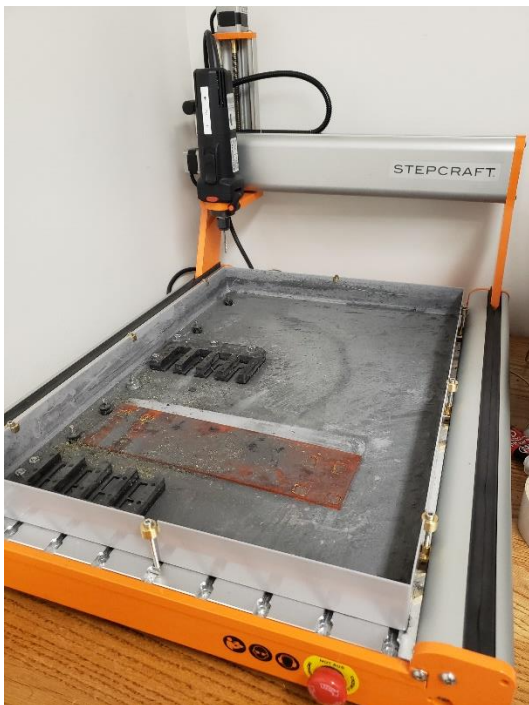


Figure 62: STEP-CRAFT CNC



Figure 63: RIGID Wet Tile Saw

Chapter 7 Future Work

7.1 Telescoping Support Tube

Commercial-off-the-shelf telescoping tubes are available for purchase from online retailers [40]. Utilizing these cylindrical telescoping tubes in the lower leg assembly of an ankle exoskeleton could allow for rapid height adjustment of the shank interface and improve rotational stiffness compared to square tubing. These outcomes have the potential to reduce the burden of clinical researchers and reduce shank interface rotation, respectively.



Figure 64: telescoping carbon fiber tubes

Potential challenges involved in implementing this change result from the need to modify the design of the lower leg assembly for compatibility with cylindrical rather than square tubing. A potential strategy for addressing these challenges is utilizing 3D printed adapter components. These components would have a curved surface for interfacing with the cylindrical tube and a flat surface for interfacing with existing lower leg components such as bearings, Bowden cable brackets, and the shank interface. However, the inclusion of these adapter components would increase distal mass of the exoskeleton system. Subsequently, a determination would have to be

made whether the increased distal mass is an acceptable trade for the decreased shank interface height adjustment effort and increased rotational stiffness.

7.2 Quick-Disconnect Bowden Cable

In order to change the length of the Bowden cable in the exoskeleton device presented in this thesis, the steel wire must be cut, and the Bowden cable exchanged. This process is both time consuming and wasteful. If features were implemented which allowed the Bowden cable and steel wire to be removed laterally, while keeping them intact, this Bowden cable exchange process could be greatly simplified, and exoskeletons more easily sized. Correctly sized Bowden cable reduces inordinate cable curvature and associated increases in friction and inefficiencies [41]. A potential design approach to implementing this quick-disconnect capability would be modifications to the ankle pulley as well as the Bowden cable brackets in the motor assembly and lower leg assembly. These modifications would introduce channels which would allow clearance for the removal of the steel wire laterally out of the components. While in use, these channels could be structurally supported by bolts orthogonal to the channels.

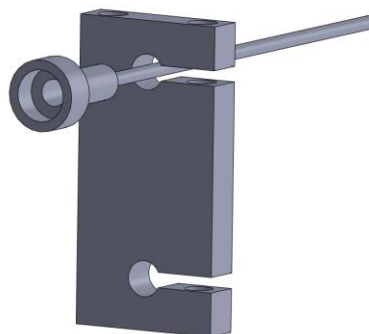


Figure 65: quick-disconnect bracket mock-up

7.3 Alternative Carbon Fiber Layup Methods

7.3.1 Prepreg Carbon Fiber

Prepreg is a type of fabric which has been pre-impregnated with resin [42]. Utilizing prepreg carbon fiber rather than a wet layup method could have the potential benefits of reduced waste, layup time, and machining time, as well as improved component strength to weight ratios for the shank interface and footplate components presented in this thesis. Potential drawbacks of this process change involve modification to the vacuum bagging and curing process. Widely available COTS vacuum bags are not feasible for use in the curing process, as they are not rated to withstand the elevated temperatures required to cure prepreg carbon fiber. Consequently, custom vacuum bags would need to be fabricated for each layup, introducing additional time to the layup process as well as potentially increasing the risk of vacuum bag pressure loss. Finally, prepreg fabric must be kept at low temperatures to preserve shelf life, necessitating the purchase of a freezer.

7.3.2 Vacuum Infusion Layup

Vacuum infusion is a process which utilizes a vacuum to pull epoxy through dry carbon fiber fabric [43]. The benefits of this method compared to conventional vacuum bagging is improved strength to weight ratio resulting from excess epoxy minimization. Potential challenges of this method are associated with the infusion setup. This process would require additional equipment such as new component molds, resin feed lines, and a resin trap to capture excess epoxy. Finally, the infusion process requires a robust seal to maintain pressure, which may be difficult to consistently achieve for each layup.

Chapter 8 Conclusions

The primary goal of this thesis was to present the mechanical design, validation, and manufacture of an optimized ankle exoskeleton for use in clinical studies. The validation section showed that the optimized device achieved desired performance in mass, torque tracking, ergonomics, and durability. These results serve as a strong positive indicator that the optimized device will be useful in studies aimed at benefiting people with walking impairment.

The optimized device had the least distal mass of any exoskeleton examined in this thesis, at just 385 grams per leg, despite requiring a high degree of strength and rigidity in the lower leg assembly due to the use of lateral support structures. Torque tracking results showed significant improvement compared to the original Lerner exoskeleton device. A 17% reduction in RMSE was found between the average error value of the original device and the optimized device operating at the original device maximum of 20 Nm. Finally, the device was found to be comfortable and reliable for extended walk times.

These results were supported by design features such as extensive use of lightweight, strong, and stiff carbon fiber components, Bowden cable force transmission, unique footplate and ankle pulley geometries, and carbon fiber reinforced 3D-printed components. Several design features presented in this thesis are novel in exoskeleton research. Subsequently, their presentation here may serve as a useful resource for future design efforts in this field.

The manufacturing section demonstrates the utility of fiber reinforced additive manufacturing, desktop CNC devices, and out of autoclave carbon fiber layup utilizing COTS vacuum bags and 3D printed molds. These methods allowed for the rapid fabrication of high-quality custom

components in limited facilities. As many research grade exoskeletons are manufactured under similar circumstances, these methods may be useful for other researchers in this field. Similarly, the content provided in the future optimizations section of this thesis may serve as an additional, useful resource.

References

- [1] M. Aisen et al., "Cerebral palsy: clinical care and neurological rehabilitation", *The Lancet Neurology*, vol. 10, no. 9, pp. 844-852, 2011. Available: 10.1016/s1474-4422(11)70176-4
- [2] P. W. Duncan, K. J. Sullivan, A. L. Behrman, S. P. Azen, S. S. Wu, S. E. Nadeau, B. H. Dobkin, D. K. Rose, J. K. Tilson, S. Cen, S. K. Hayden; LEAPS Investigative Team, Body-weight–supported treadmill rehabilitation after stroke. *N. Engl. J. Med.* 364, 2026–2036 (2011).
- [3] Cruz, M. D. Lewek, Y. Y. Dhaher, Biomechanical impairments and gait adaptations post-stroke: Multi-factorial associations. *J. Biomech.* 42, 1673–1677 (2009).
- [4] D. B. Maltais, M. R. Pierrynowski, V. A. Galea, and O. Bar-Or, "Physical activity level is associated with the O₂ cost of walking in cerebral palsy," *Med. Sci. Sports Exerc.*, vol. 37, no. 3, pp. 347–353, 2005.
- [5]. S. A. Combs, M. Van Puymbroeck, P. A. Altenburger, K. K. Miller, T. A. Dierks, A. A. Schmid, Is walking faster or walking farther more important to persons with chronic stroke? *Disabil. Rehabil.* 35, 860–867 (2013).
- [6] N. E. Mayo, S. Wood-Dauphinee, S. Ahmed, C. Gordon, J. Higgins, S. McEwen, N. Salbach, Disablement following stroke. *Disabil. Rehabil.* 21, 258–268 (1999).
- [7] Z. Lerner et al., "An Untethered Ankle Exoskeleton Improves Walking Economy in a Pilot Study of Individuals With Cerebral Palsy", *IEEE Transactions on Neural Systems and Rehabilitation Engineering*, vol. 26, no. 10, pp. 1985-1993, 2018. Available: 10.1109/tnsre.2018.2870756.

- [8] L. M. Mooney, E. J. Rouse, and H. M. Herr, "Autonomous exoskeleton reduces metabolic cost of human walking during load carriage," *Journal of NeuroEngineering and Rehabilitation*, vol. 11, no. 1, p. 80, 2014.
- [9] L. N. Awad, J. Bae, K. O'Donnell, S. M. M. D. Rossi, K. Hendron, L. H. Slood, P. Kudzia, S. Allen, K. G. Holt, T. D. Ellis, and C. J. Walsh, "A soft robotic exosuit improves walking in patients after stroke," *Science Translational Medicine*, vol. 9, no. 400, 2017.
- [10] B. C. Conner, J. Luque, and Z. F. Lerner, "Adaptive Ankle Resistance from a Wearable Robotic Device to Improve Muscle Recruitment in Cerebral Palsy," *Annals of Biomedical Engineering*, vol. 48, no. 4, pp. 1309–1321, 2020.
- [11] D. L. Damiano, K. E. Alter, and H. Chambers, "New clinical and research trends in lower extremity management for ambulatory children with cerebral palsy," *Phys. Med. Rehabil. Clinics*, vol. 20, no. 3, pp. 469–491, 2009.
- [12] Y. L. Kerkum, A. I. Buizer, J. C. van den Noort, J. G. Becher, J. Harlaar, and M.-A. Brehm, "The effects of varying ankle foot orthosis stiffness on gait in children with spastic cerebral palsy who walk with excessive knee flexion," *PLoS ONE*, vol. 10, no. 11, p. e0142878, 2015.
- [13] A. Vistamehr, S. A. Kautz, R. R. Neptune, "The influence of solid ankle-foot-orthoses on forward propulsion and dynamic balance in healthy adults during walking." *Clin. Biomech.* 29, 583–589 (2014).

- [14] Anttila, H., I. Autti-Raïmoï , J. Suoranta, M. Maïkelaï , and A. Malmivaara. Effectiveness of physical therapy interventions for children with cerebral palsy: a systematic review. *BMC Pediatr.* 8:14, 2008.
- [15] K. A. Witte, J. Zhang, R. W. Jackson, and S. H. Collins, "Design of two lightweight, high-bandwidth torque-controlled ankle exoskeletons," *2015 IEEE International Conference on Robotics and Automation (ICRA)*, 2015.
- [16] W. van Dijk, C. Meijneke and H. van der Kooij, "Evaluation of the Achilles Ankle Exoskeleton", *IEEE Transactions on Neural Systems and Rehabilitation Engineering*, vol. 25, no. 2, pp. 151-160, 2017. Available: 10.1109/tnsre.2016.2527780.
- [17] J. Bae, C. Siviyy, M. Rouleau, N. Menard, K. Odonnell, I. Geliana, M. Athanassiu, D. Ryan, C. Bibeau, L. Sloom, P. Kudzia, T. Ellis, L. Awad, and C. J. Walsh, "A Lightweight and Efficient Portable Soft Exosuit for Paretic Ankle Assistance in Walking After Stroke," *2018 IEEE International Conference on Robotics and Automation (ICRA)*, 2018.
- [18] K. Langlois, M. Moltedo, T. Bacek, C. Rodriguez-Guerrero, B. Vanderborght and D. Lefeber, "Design and Development of Customized Physical Interfaces to Reduce Relative Motion Between the User and a Powered Ankle Foot Exoskeleton", *2018 7th IEEE International Conference on Biomedical Robotics and Biomechatronics (Biorob)*, 2018. Available: 10.1109/biorob.2018.8487706
- [19] A. J. Young and D. P. Ferris, "State of the Art and Future Directions for Lower Limb Robotic Exoskeletons," *IEEE Transactions on Neural Systems and Rehabilitation Engineering*, vol. 25, pp. 171–182, Feb. 2017.

- [20] S. Collins, M. Wiggin and G. Sawicki, "Reducing the energy cost of human walking using an unpowered exoskeleton", *Nature*, vol. 522, no. 7555, pp. 212-215, 2015.
- [21] M. Wiggin, G. Sawicki and S. Collins, "An exoskeleton using controlled energy storage and release to aid ankle propulsion", *2011 IEEE International Conference on Rehabilitation Robotics*, 2011.
- [22] P. Kedem and D. Scher, "Evaluation and management of crouch gait", *Current Opinion in Pediatrics*, vol. 28, no. 1, pp. 55-59, 2016.
- [23] L. N. Awad, J. Bae, K. Odonnell, K. L. Hendron, L. Sloom, C. Siviy, P. Kudzia, T. D. Ellis, and C. J. Walsh, "Soft exosuits increase walking speed and distance after stroke," *2017 International Symposium on Wearable Robotics and Rehabilitation (WeRob)*, 2017.
- [24] L. Sloom, J. Bae, L. Baker, K. O'Donnell, N. Menard, F. Porciuncula, D. Choe, T. Ellis, L. Awad, and C. Walsh, "O 089 - A soft robotic exosuit assisting the paretic ankle in patients post-stroke: Effect on muscle activation during overground walking," *Gait & Posture*, 2018.
- [25] L. M. Mooney, E. J. Rouse, and H. M. Herr, "Autonomous exoskeleton reduces metabolic cost of walking," *2014 36th Annual International Conference of the IEEE Engineering in Medicine and Biology Society*, 2014.
- [26] R. C. Browning, J. R. Modica, R. Kram, and A. Goswami, "The Effects of Adding Mass to the Legs on the Energetics and Biomechanics of Walking," *Medicine & Science in Sports & Exercise*, vol. 39, no. 3, pp. 515–525, 2007.

[27] D. P. Ferris, G. S. Sawicki, and M. A. Daley, "A Physiologists Perspective On Robotic Exoskeletons For Human Locomotion," *International Journal of Humanoid Robotics*, vol. 04, no. 03, pp. 507–528, 2007.

[28] J. Lehmann, R. Price, R. Okumura, K. Questad, B. de Lateur and A. Négretot, "Mass and mass distribution of below-knee prostheses: Effect on gait efficacy and self-selected walking speed", *Archives of Physical Medicine and Rehabilitation*, vol. 79, no. 2, pp. 162-168, 1998. Available: 10.1016/s0003-9993(98)90293-3.

[29] T. Huang and A. Kuo, "Mechanics and energetics of load carriage during human walking", *Journal of Experimental Biology*, vol. 217, no. 4, pp. 605-613, 2013. Available: 10.1242/jeb.091587 [Accessed 16 March 2020].

[30] R. W. Jackson and S. H. Collins, "An experimental comparison of the relative benefits of work and torque assistance in ankle exoskeletons," *J. Appl. Physiol.*, vol. in review, 2015.

[31] J. M. Donelan, R. Kram, and A. D. Kuo, "Mechanical and metabolic determinants of the preferred step width in human walking." *Proc. Roy. Soc. Lon. B*, vol. 268, pp. 1985–1992, 2001

[32] PatriotMobilityINC, "New Exoskeleton Design Helps Handicap Accessibility," *Mobile You Magazine*, 22-May-2015. [Online]. Available:

<https://themobileyou.wordpress.com/2015/04/16/new-exoskeleton-design-helps-handicap-accessibility/>.

[33] P. Malcolm, R. E. Quesada, J. M. Caputo, and S. H. Collins, "The influence of push-off timing in a robotic ankle-foot prostheses on the energetics and mechanics of walking," vol. 12, no. 21, p. in press, 2014.

[34] G. Orekhov, Y. Fang, J. Luque, and Z. F. Lerner, "Ankle Exoskeleton Assistance Can Improve Over-Ground Walking Economy in Individuals With Cerebral Palsy," *IEEE Transactions on Neural Systems and Rehabilitation Engineering*, vol. 28, no. 2, pp. 461–467, 2020.

[35] "Engineering Materials," *Engineering ToolBox*. [Online]. Available: https://www.engineeringtoolbox.com/engineering-materials-properties-d_1225.html.

[36] "Standard Modulus Carbon," *Rock West Composites*. [Online]. Available: <https://www.rockwestcomposites.com/shaped-tubing/square-tubing/standard-modulus-carbon>.

[37] L.-F. Yeung, C. Ockenfeld, M.-K. Pang, H.-W. Wai, O.-Y. Soo, S.-W. Li, and K.-Y. Tong, "Design of an exoskeleton ankle robot for robot-assisted gait training of stroke patients," *2017 International Conference on Rehabilitation Robotics (ICORR)*, 2017.

[38] "Learning Center - Vacuum Bagging Equipment & Techniques for Room-Temp Applications," *Fibre Glast*. [Online]. Available: https://www.fibreglast.com/product/vacuum-bagging-equipment-and-techniques-for-room-temp-applications/Learning_Center.

[39] S. Black, "Abrasive machining methods for composites," *CompositesWorld*. [Online]. Available: <https://www.compositesworld.com/articles/abrasive-machining-methods-for-composites>.

[40] "Carbon Fiber Telescoping Tubes," *DragonPlate*. [Online]. Available:

<https://dragonplate.com/carbon-fiber-telescoping-tubes>.

[41] D. Chen, Y. Yun, and A. D. Deshpande, "Experimental characterization of Bowden cable friction," *2014 IEEE International Conference on Robotics and Automation (ICRA)*, 2014.

[42] "Learning Center - About Prepregs," *Fibre Glast*. [Online]. Available:

https://www.fibreglast.com/product/about-prepregs/Learning_Center.

[43] "Learning Center - Vacuum Infusion - The Equipment & Process of Resin Infusion

Brochure," *Fibre Glast*. [Online]. Available: https://www.fibreglast.com/product/vacuum-infusion-Guide/Learning_Center.